LA-UR-14-20441
Approved for public release; distribution is unlimited.

Title:	Physical Uncertainty Bounds (PUB)
Author(s):	Vaughan, Diane Elizabeth Preston, Dean L.
Intended for:	White Paper
Issued:	2015-03-19 (rev.2)

LA-UR-14-20441

Physical Uncertainty Bounds (PUB)

Diane E. Vaughan* and Dean L. Preston

Computational Physics Division, MS F644
Los Alamos National Laboratory
Los Alamos, NM 87545, USA
LA-UR-14-20441

Sept 8, 2014

*E-mail: dev@lanl.gov

Acknowledgements

We would like to extend special thanks Tim Trucano (Sandia), Scott Doebling (LANL) and Bob Webster (LANL) for their extensive editing of this paper and Mark Anderson (LANL) who gave the first external talk on Physical Uncertainty Bounds (PUB) at the ASME V&V Symposium. We have been fortunate to have received input in the form of discussions and edits from the following list of scientists. We could not have finished this paper without this input.

Marvin Adams, Texas A&M
Frank Alexander, LANL, CCS-DO
Mark Anderson, LANL, XCP-DO
Bill Archer, LANL, ADX
Lowell Brown, LANL, XCP-4
Kevin Buescher, LANL, XCP-8
Mark Chadwick, LANL, ADX
James Cooley, LANL, CCS-2
Scott Doebling, LANL, XCP-8
Andrew Fraser, LANL, XCP-8
Nick Hengartner, LANL, T-6
James Howse, LANL, CCS-3
Jim Kamm, LANL, XCP-4
Len Margolin, LANL, XCP-4
Garry Maskaly, LANL, XTD-PRI
Charlie Nakhleh, LANL, XTD-DO
Denise Neudecker, LANL, T-2
Bill Rider, Sandia
Don Sandoval, LANL, XTD-PRI
John Scott, LANL, XTD-IDA
Gowri Srinivasan, LANL, T-5
Sky Sjue, LANL, P-21
Patrick Talou, LANL, T-2
Tim Trucano, Sandia
Bob Webster, LANL, ADX
Morgan White, LANL, XCP-5

Abstract

This paper introduces and motivates the need for a new methodology for determining upper bounds on the uncertainties in simulations of engineered systems due to limited fidelity in the composite continuum-level physics models needed to simulate the systems. We show that traditional uncertainty quantification methods provide, at best, a lower bound on this uncertainty. We propose to obtain bounds on the simulation uncertainties by first determining bounds on the physical quantities or processes relevant to system performance. By bounding these physics processes, as opposed to carrying out statistical analyses of the parameter sets of specific physics models or simply switching out the available physics models, one can obtain upper bounds on the uncertainties in simulated quantities of interest.

Contents

1. Introduction 4
2. Physics categories: five examples 12
   2.1 Physics category: plasma fusion reactions 12
   2.2 Physics category: material damage 13
   2.3 Physics category: neutronics 15
   2.4 Physics category: material strength 17
   2.5 Physics category: HE 19
3. Why are we not using parametric or model selection methodologies to bound the uncertainty? 20
   3.1 Parametric methodologies for uncertainty quantification are not applicable to physics models 20
      3.1.1 Some models have no (or almost no) parameters 22
      3.1.2 Model approximations and assumptions 24
      3.1.3 There are no parameters for regimes with no data 27
      3.1.4 Parameters are designed to capture mean behavior 29
   3.2 Combined model selection and parametric methodologies 29
      3.2.1 Combined methodologies provide only lower bounds on uncertainty 30
4. Physical uncertainty bounds 32
   4.1 Material damage 33
   4.2 Strain to fracture 33
   4.3 Shear modulus 33
   4.4 Melt temperature 33
   4.5 Flow stress 34
5. Concluding remarks 34
6. Appendix A 34
   References 35

1 Introduction

There is a great deal of literature on the quantification of uncertainty in many fields. Much of the literature focuses on specific applications, while some is aimed at defining terminology that can be applied across fields. We have found that subtle differences in terminology can lead to immense confusion and misunderstandings. Therefore, we carefully define our terminology at the outset, that is, in the following paragraphs. Rather than add to the existing definitions, when possible, we will use terminology from two sources, a report by the National Research Council (NRC) [1] and a paper by Trucano [2]. The applications under consideration in these two sources are closely related to our discussion and they each contain terminology that allows us to articulate our points. We formulate new terminology only where necessary. For the aid of the reader, when a term is defined, we italicize it.

In the words of the NRC committee on Mathematical Foundations of Verification, Validation, and Uncertainty Quantification, *Uncertainty Quantification* should address the question: "How do the various sources of error and uncertainty feed into uncertainty in the model-based prediction of the quantities of interest?"[1]. By model-based prediction the committee is referring to a computational model that is used to simulate a real-world physical system (e.g., a bridge, protein folding, the climate), but they limit their focus to physics based and engineering models. Likewise, this paper focuses only on computational models of engineered systems (e.g., a bridge, a plate impact experiment (flyer plate)). The conclusions we draw may pertain to other fields, but we make no such claim. In particular, this paper is about the uncertainty associated with a quantity of interest from a simulation of an engineered system due to using physics models to approximate physics processes in the simulation.

A *physics process* is a relation between two or more physical quantities, e.g. the rate at which plasma

ion and electron temperatures equilibrate as a function of the individual temperatures, particle masses, and number densities. Note that a physics process need not be time dependent, e.g. the shear modulus as a function of temperature and density. A *physics model* is an approximate mathematical representation of a physics process. As an example of a physics model, consider the plastic constitutive relation of a metal. This relates the basic quantities governing plastic deformation, e.g. the flow stress, plastic strain, strain rate, temperature, and density. It is an approximate representation of the very complicated mesoscale physics responsible for the flow of a solid, and is therefore a physics model. In contrast, a result obtained from experimentally validated fundamental theory without making any (significant) approximations is not, by our definition, a physics model. A physics law is a relation for which we believe that further experiments cannot refute its applicability in the domain of application. For example, the time required for a ball bearing to fall a distance d in vacuum if dropped with zero initial velocity is $t = \sqrt{2\,d/g}$, where g is the acceleration due to gravity. This result follows directly from the fundamental *physics law* $\mathbf{F} = \mathrm{m}\mathbf{a}$, hence it is not a physics model. In essence, *physics laws* could be defined as *physics models* to which we ascribe no uncertainty in accuracy. However, to keep the distinction clear we avoid this definition.

It is typically the case that several physics models exist for a given physics process. Those models differ in the sets of approximations and assumptions that underly them. In computational models, physics models are combined with physics laws (mass conservation, energy conservation, ...) to simulate engineered systems.

Consider the set of all physical quantities $\{q_i\}$, $i = 1, \ldots, N$, pertinent to the performance (dynamics) of a given engineered system. These quantities may be grouped into *physics categories*, each of which is comprised of one or more physics processes. Note that a physics process may belong to one or more physics categories. Examples of physics categories include, but are not limited to, plasma fusion, material strength, neutronics, material damage, equations of state (EOS) for metals and alloys, EOSs for plasmas and warm dense matter, and high explosive (HE) burn and EOS. The definition of a physics category is often a matter of convention, but the definition can be made precise, as is provided in Appendix A.

We found it necessary to define physics categories in this paper for three reasons. First, the individual physics categories provide a framework for the description in Section 2 of the physics processes and corresponding physics models required to understand this paper. Second, the breakdown of the physics categories into their respective physics processes shows that, in general, a large number number of physics models and respective parameters are required to model even the simplest of engineered systems, hence, one cannot determine the uncertainty associated with a physics category (e.g., material strength) by considering just one of its physics processes (e.g., flow stress); this generally results in an underestimate of the uncertainty in a simulated quantity of interest. Third, input files that contain simulation specifics (geometry, materials, material models, etc.) are often organized by physics categories.

We now rephrase the above quote from the committee on Mathematical Foundations of Verification, Validation, and Uncertainty Quantification [1] using our terminology to more specifically define the *Uncertainty Quantification* question we are addressing: How do the various sources of error and uncertainty due to using physics models to approximate physics processes feed into the uncertainty in the simulation-based prediction of the quantities of interest? Note that we have used the terminology "simulation-based" instead of "model-based." Throughout this paper the word "model" will mean "physics model", not "numerical simulation model." Understanding how to address this uncertainty will aid in:
1. Determining resource allocation. In particular, for which physics processes and in what regimes would experimental evidence or better theoretical models reduce our uncertainty? 2. Quantifying the uncertainty due to limited fidelity of physics models on our ability to predict experiments with no previous experiments to baseline against.

The reader with a background in uncertainty quantification might refer to the uncertainty discussed in this paper as model-form uncertainty. We address only a subset of model-form uncertainty as defined in [1] and [2]. In particular, in [1] the use of subgrid models that do not possess the full symmetry group of the Navier-Stokes equations is presented as an example of model-form error. In contrast, we do not consider uncertainties associated with numerical methods. Our discussion is limited to physics models as defined above. Similarly, [2] includes numerical models (e.g., artificial viscosity) in the model-form uncertainty. Although, there are certainly valid arguments for including numerical models in a definition of physics models, we have not done so. As stated in [1],"Methods for expressing model-form error, and assessing its impact on prediction uncertainty, are in their infancy compared to methods for addressing parametric methods." We emphasize that this paper addresses only a subset of the model-form error as described in [1] and [2].

From the literature we have selected nineteen physics models from five physics categories (plasma

fusion, material damage, neutronics, material strength, and high explosives) to illustrate our main points. Our examples will show that an individual physics category generally includes several physics processes. Therefore, composite continuum-level physics models are required to model a physics category. The primary purpose of this paper is to motivate the need for a new methodology for determining upper bounds on the uncertainties in simulations of engineered systems due to limited fidelity in the composite continuum-level physics models needed to simulate the systems. The last Section of the paper introduces the new methodology and outlines how this methodology is currently being implemented for 5 physics processes.

This paper is general in that it is not concerned with any particular simulation paradigm or engineered system. Simulation of the performance of a given engineered system requires a set of physics models associated with one or more physics categories. Examples of engineered systems include, but are not limited to, conventional ordnance, dynamic materials experiments, inertial confinement fusion (ICF) capsules, and critical assemblies. Engineered systems that involve the fewest physics categories are highly sought after as they are the experimental base for parameter calibration. Considerable effort is put into the design and execution of these focused experiments. Few exist that entail only one physics category. Rather, it is generally the case that an experiment designed to probe a particular physics category also involves several additional physics categories. For example, a simulation of damage development in a metal necessarily involves an EOS and a material strength model.

We propose obtaining bounds on simulation uncertainties by first determining bounds on the physical quantities or processes (independent of any particular physics theoretical model) relevant to system performance. As discussed above, these physical quantities/processes can be grouped into physics categories. It is these individual physical quantities and physics processes for which we have theoretical physics models, and these models collectively constitute a composite physics model for the given category. We propose bounding these physics processes themselves as opposed to carrying out statistical analyses of the parameter sets of specific physics models (parametric methodologies) or simply switching out the available physics models (model selection methodologies). The difference between our proposed approach, which is based on bounding the physics processes, and parametric methodologies will be mathematically defined later in this Introduction. This approach constitutes a significant advance over traditional parametric methodologies which we will show provide at best *lower* bounds on the physics category uncertainties. The methodology advocated here has the potential to provide, for the first time, realistic bounds on the performance of engineered systems.

In each physics category there are, in general, several composite physics models available to the user. Each composite model for the given physics category is comprised of one or more physics models. All of these interrelated models are required to compute the physical quantity that defines the physics category. Each of the physics models in a composite model may in turn be composed of sub-models. This is often necessary because a given physics model typically involves multiple complex physical processes spanning a broad range of length and time scales. For example, a metal EOS includes sub-models for the zero-temperature isotherm (cold curve), the melt curve, the electron-thermal contribution, etc. A specific EOS might utilize an analytic cold curve, Lindemann melt, a Thomas-Fermi-Dirac (TFD) electron-thermal contribution, a LANL standard Gruneisen gamma, etc.; alternatively, the EOS sub-models might include an *ab initio* cold curve, a quantum-molecular-dynamics (QMD) melt curve, an Inferno model electron-thermal contribution [18], and a Burakovsky-Preston (BP) Gruneisen parameter [19].

Although much of the physics of a physics category may be known from experiment, basic theory, or simulations, and is accurately represented (modeled), it is typically the case that some of the physics is not. The uncertainties can be very large when theoretical difficulties are coupled to a lack of both experimental and numerical data. In this case, a traditional parametric methodology, involving as it often does the determination of a posterior (probability distribution of model parameters) through comparisons with data, cannot be meaningfully carried out. Generally, the physics process uncertainty is dominated by a small subset of the sub-models of which it is comprised and the uncertainty in those sub-models is often large only over limited regimes. In other words, it is usually just a few pieces of the physics that are responsible for most of the uncertainty, and it is primarily this physics which limits the reliability of our simulations. We need bounds on the uncertainty associated with this physics. Even though theory may not be good enough to yield an accurate sub-model, it can nevertheless be relied upon to provide bounds on the uncertainty in the physics of that sub-model, or the full model. For example, the flow stress of a metal at high plastic strain rates can be bounded by accounting for extremes in dislocation density, the dislocation drag coefficient, and demanding continuity of the rate sensitivity as the strain

rate is increased above the rates accessible by current measurement techniques.

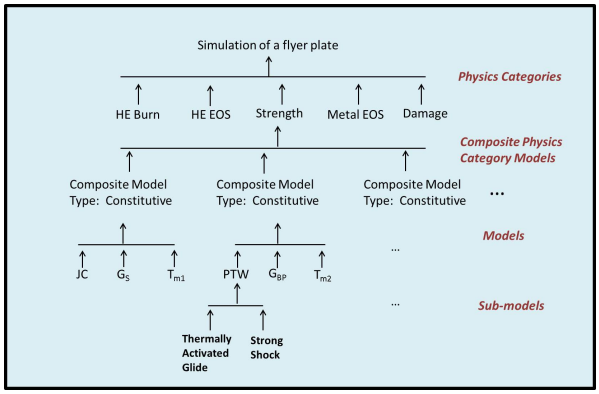

Figure 1: Physics categories for an explosively driven flyer. For illustration purposes, the material strength category is broken down.

Figure 1 shows the physics categories and illustrates the breakdown of composite models into physics models (approximate representations of physics processes) and sub-models for a numerical simulation of an explosively driven flyer (HE and two metals). Relevant physics categories include HE, metal EOS, material strength, and material damage. For each physics category a composite continuum-level physics category model needs to be selected. For illustration purposes, one of the five physics categories, material strength, is broken down. A composite strength model may include the Preston-Tonks-Wallace (PTW) plastic constitutive relation [20], the Straub shear modulus [21], and the Burakovsky-Greeff-Preston (BGP) melt temperature model [22]. The PTW model is comprised of two sub-models: a low-strain-rate sub-model representing thermally activated dislocation glide, and a high-strain-rate sub-model based on Wallace's theory of overdriven shock waves in metals [23].

Some sub-models represent processes that are well-described by established theory, hence the corresponding sub-model is obtained by giving specific values to quantities appearing in a general theory. In contrast, some, and usually most, of the processes are not reliably described by any existing theory, in which case there are several possible routes to a sub-model. The sub-model may be constructed by fitting to experimental data, but because of the difficulty discussed above in developing focused experiments that isolate individual physics categories, and the extreme pressures, temperatures, and spatio-temporal scales involved in some modeling efforts, experimental data are frequently non-existent. Large scale, eventually exascale, computations, e.g. MD and QMD simulations, can be carried out to provide numerical data when the experimental variety is unavailable. [1] And of course a sub-model might be constructed by following the usual approach of the theoretical physicist, namely, idealize the physics, that is, make simplifications and approximations to render the mathematical representation of a complex physical system tractable. Physics models, as approximate mathematical representations of physics processes, are generally functions over a continuous parametric space. Specifically, let $\{q_i\}$, $i = 1, \ldots, N$, be a set of physical quantities, one of which, say q_N, is approximated, $\hat{q}_N$, with a physics model as a function of $q_1, \ldots, q_{N-1}$, which are coordinates of R^{N-1}, and a set of parameters, $\{p_j\}$, $j = 1, \ldots, M$, which are likewise coordinates in R^M. A physics model, $\mathcal{M}$, for a physics process, may be expressed as

$$\hat{q}_N = \mathcal{M}\left(\{q_1, \ldots, q_{N-1}\}, \{p_j\}, \{m_k\}\right) , \tag{1}$$

where the $\{m_k\}$ are physical quantities that must be obtained from other physics models. For instance, the strain, q_1, strain rate, q_2, temperature, q_3, and melt temperature, m_1, dependence of flow stress $q_4 = q_N$ is a physics process for which their are many theoretical approximate models (e.g., PTW=$\mathcal{M}_{PTW}$). Note that the pressure dependence of melt temperature is a physics process itself for which many models exist. A physics model is constructed using some combination of experimental data on q_N, numerical simulation data on q_N, and approximate theoretical representations of the dependence of q_N on $q_1, \ldots, q_{N-1}$, each over limited ranges of the $q_1, \ldots, q_{N-1}$. Therefore, the model is applicable only on a submanifold of R^{N-1} which will be called $\mathcal{Q}$. The q_N data have associated error bars, and in regimes where there are no data,

[1] The authors are currently carrying out quantum MD calculations to provide numerical data for some of the bounds presented in Section 7.

q_N can be bounded on the basis of theoretical understanding of the physics process. The bounds on q_N are assumed (convenient, but not necessary) to be symmetric about a central value, $\bar{q}_N(q_1, \ldots, q_{N-1})$; the error is denoted $\delta q_N(q_1, \ldots, q_{N-1})$. We define the N-dimensional manifold

$$\mathcal{Y} = \{(q_1, \ldots, q_N) \,|\, \bar{q}_N - \delta q_N < q_N < \bar{q}_N + \delta q_N \,, (q_1, \ldots, q_{N-1}) \in \mathcal{Q}\} \;; \tag{2}$$

$\mathcal{Y}$ is the set of all q_N tuples over $\mathcal{Q}$ and within the bounds.

In Figure 2 we illustrate these definitions using a physics model, $\mathcal{M}$, and the physics process Finite T Shear (temperature dependence, q_1, of the shear modulus, $q_2 = q_N$) that will be explained in detail in Sections 2.4 and 3.2.

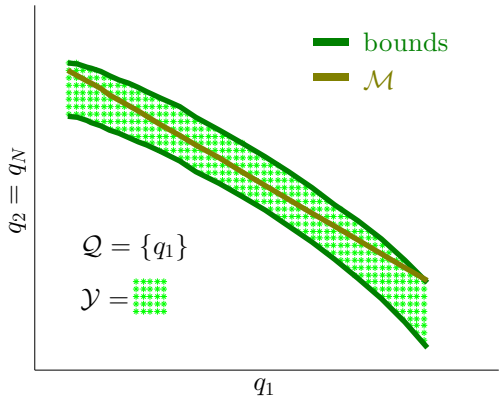

Figure 2: Schematic of a physics process for which we have "hard" bounds, that is, fundamental physics tells us that the "true" physics process relation lies within $\mathcal{Y}$.

This physics process is uncommon in that one physical quantity is a function of only one other physical quantity, and just one parameter:

$$\hat{q}_N = \hat{q}_2 = \mathcal{M}\left(\{q_1\}, \{p_1\}\right) . \tag{3}$$

This model is based on a simple approximation, namely, $\hat{q}_2$ is linear in q_1. For these reasons, this physics model is the simplest example we could find to use for illustration purposes in this Introduction. There is uncertainty associated with the determination of the parameter, p_1. The uncertainty in simulating an engineered system involving $\hat{q}_2$ could be approximately determined by forward propagating a set of parameter variations that do not violate the bounds. Figure 3 (left) is a schematic of the parameter variations that obey the bounds. These parameter variations define a manifold $\hat{\mathcal{Y}}$ that is contained in $\mathcal{Y}$, that is, $\hat{\mathcal{Y}} \subset \mathcal{Y}$. Therefore, $\hat{\mathcal{Y}}$ represents the union of the range of all parametric variations of the physics model.

Consider the case that $\mathcal{M}$ is a physics law, $\mathcal{L}$, that is, $\mathcal{L}$ follows rigorously from established, fundamental physics. In principle, the parameters can be expressed in terms of fundamental physical quantities. For $\mathcal{M} = \mathcal{L}$, there must exist a set of parameters, $\{\bar{p}_j\}$, such that $\hat{q}_N(\{q_i\}, \{\bar{p}_j\}) = q_N$ and necessarily $\hat{\mathcal{Y}} \subseteq \mathcal{Y}$, i.e., the true physics process lies within the set of allowed parametric variations. Moreover, $\hat{\mathcal{Y}}$ would be an *upper* bound on the model fidelity uncertainty, which is clearly not the case in our example. If distributions between the bounds were known then the functional form of $\mathcal{L}$ could be used to find a manifold $\hat{\mathcal{X}}$, such that $q_N = \hat{q}_N \subseteq \hat{\mathcal{X}} \subseteq \hat{\mathcal{Y}} \subseteq \mathcal{Y}$, generally a smaller upper bound on the model fidelity uncertainty.

As an interesting special case of $\mathcal{M} = \mathcal{L}$, assume $\mathcal{L}$ is a materials model for a particular alloy that exhibits small but significant compositional variations with a known continuous distribution. The model (physics law) provides an exact representation of the modeled material propoerty, q_N, for each compositional variation with a unique set of parameter values. Assuming no experimental error, $\mathcal{Y}$ would be the set of all realizations of q_N over the distribution of compositions, parametric variations must span $\mathcal{Y}$, hence $\hat{\mathcal{Y}} = \mathcal{Y}$, and moreover, $\hat{\mathcal{X}} = \hat{\mathcal{Y}}$. Allowing for experimental error, $\mathcal{Y}$ expands along q_N, and we have $\hat{\mathcal{X}} = \hat{\mathcal{Y}} \subset \mathcal{Y}$.

In contrast, if $\mathcal{M}$ is a physics model it is, by definition, an approximation to the physics and therefore $\hat{q}_N \neq q_N$ for all $\{p_j\}$ and $\hat{\mathcal{Y}}$ is, at best, a *lower* bound on the uncertainty. Moreover, using the functional

form of $\mathcal{M}$ to reduce this uncertainty replaces the already lower bound $\hat{\mathcal{Y}}$ with a potentially smaller lower bound $\hat{\mathcal{X}}$ (see the right hand side of Figure 3).

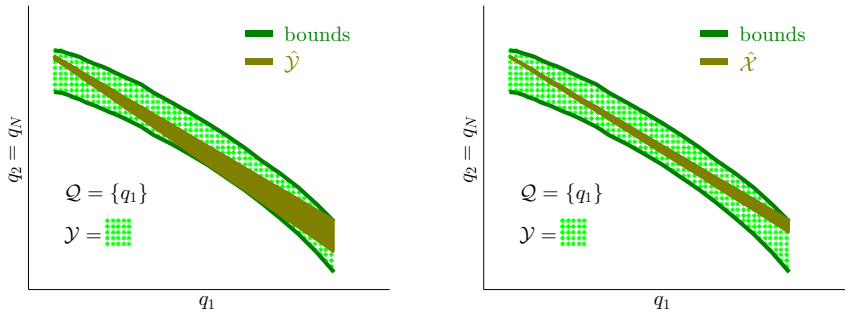

Figure 3: Bounds

The size of the lower bound $\hat{\mathcal{X}}$ depends greatly on the number of parameters in the functional form of the model, which has little, or nothing, to do with the model's fidelity at approximating the physics process. It is important to note that it is often the case that a model's fidelity over some regime is such that $\hat{\mathcal{Y}} = \emptyset$. Such models are often employed because they are the only models of a given physics process that are available (when possible, the parameters are calibrated as close to the data as possible over the appropriate regimes). When $\hat{\mathcal{Y}} = \emptyset$, parametric variations cannot be used to obtain either lower or upper bounds on the model fidelity uncertainty. In particular, a nontrivial $\hat{\mathcal{X}}$ can still be determined, but $\hat{\mathcal{X}} \not\subseteq \mathcal{Y}$. We have selected a physics process and model from Section 2 to illustrate this in Figure 4. This and many other examples of such physics processes and respective physics models will be discussed in Section 3.

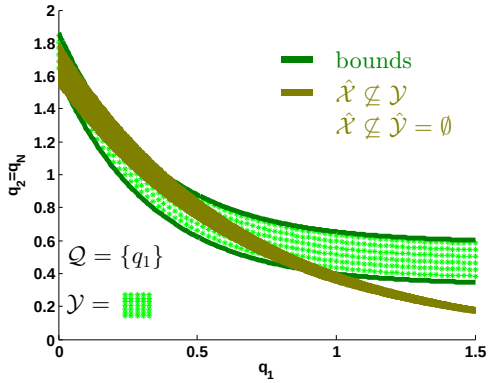

Figure 4: Schematic of a physics process and physics model for which $\hat{\mathcal{Y}} = \emptyset$ and therefore $\hat{\mathcal{X}} \not\subseteq \mathcal{Y}$.

The methodology used to quantify uncertainty should depend on the question or issue being addressed. If the issue is to determine the uncertainty in simulations of an engineered system due to our ability to fit parameters for a given physics model then forward propagation of parametric model realizations from a rigorously determined $\hat{\mathcal{X}}$ is absolutely appropriate. Moreover, parametric methodologies are the only choice for model calibration. However, parametric methods are not adequate to address questions of resource allocation (e.g., Do we need to invest in a new theoretical model, $\mathcal{M}_{new}$, of a particular physics process? Do we need more data to further constrain $\mathcal{Y}$, thereby increasing our knowledge of the functional form of the physics process?). When parametric methodologies are used to determine the uncertainty in our ability to simulate an engineered system due to our limited ability to model the relevant physics processes then they provide, at best, a lower bound on the uncertainty.

In general, physics processes are higher dimensional relationships, as are the physics models used to

approximate them. For instance, the Johnson-Cook (JC) strain-to-fracture model is

$$\epsilon_f = \left[D_1 + D_2 \exp\left(-D_3 \frac{\bar{P}}{\sigma}\right)\right] \left[1 + D_4 \ln\left(\frac{\dot{\epsilon}}{\dot{\epsilon}_0}\right)\right] (1 + D_5 T^*) \ . \tag{4}$$

In (4), ϵ_f is the fracture strain, $\dot{\epsilon}_0 = 1s^{-1}$, $\dot{\epsilon}$ is the strain rate, σ is the flow stress, $\bar{P} = -Tr\left(\boldsymbol{\sigma}\right)/3$ is the mean compressive stress (pressure), and T^* is the homologous temperature

$$T^* = \frac{T - T_{RT}}{T_m(\rho) - T_{RT}} \ , \tag{5}$$

where $T_m(\rho)$ is the melting temperature at a given density, ρ, and $T_{RT} = 298$K is room temperature. The JC strain to fracture can be expressed in the form (1):

$$\hat{\epsilon}_f = \mathcal{M}\left(\left\{\bar{P}, \sigma, \dot{\epsilon}, T, \right\}, \{D_1, D_2, D_3, D_4, D_5\}, \{T_m(\rho)\}\right) \ . \tag{6}$$

The 5-dimensional manifold $\mathcal{Y}$ for the JC model is

$$\mathcal{Y} = \left\{(\bar{P}, \sigma, \dot{\epsilon}, T, \epsilon_f) \,|\, \bar{\epsilon_f} - \delta\epsilon_f < \epsilon_f < \bar{\epsilon_f} + \delta\epsilon_f, (\bar{P}, \sigma, \dot{\epsilon}, T) \in \mathcal{Q}\right\} \ . \tag{7}$$

We define a *parametric methodology* as any methodology that relies on varying physics model parameters, $\{p_j\}$, to determine the uncertainty in the simulation-based prediction of a quantity of interest. *Model selection methodologies* determine the uncertainty in calculated system performance by switching out the available physics models. The alternative methodology we are proposing involves the determination of upper, B_U, and lower bounds, B_L, on the physical quantity q_N. We will show that bounding the physics processes has several advantages over traditional parametric and model selection methodologies:
1. Experimental uncertainties, when available, are on q_N.
2. The approximations and assumptions in physics models are on q_N and no parameters are provided by the theorists to account for the approximations and assumptions of a given model.

There are disadvantages to the proposed methodology:
1. Each physics process considered must be understood in depth. The bounds, as well as techniques for exploring the space between them, will be specific to the given physics process. In particular, no generalized black-box uncertainty quantification technique is applicable.
2. The proposed methodology cannot be carried out by modifying input decks for simulation codes. It requires modifications to simulation codes to evaluate the uncertainties.

Large suites of simulations by subject matter experts have shown that it is sometimes the case that the extremes in physics processes (the bounds) provide the extremes in our quantities of interest, in which case forward propagation of the bounds themselves is sufficient. We are now working to develop rigorous mathematical criteria to identify these cases. For instance, if it can be shown that if the quantity of interest is monotone in the integral, then forward propagating the bounds will yield the extremes in the quantity of interest. However, it is not always the case that the bounds on a physics process give the extremes of a quantity of interest. In general, we recommend forward propagation of the bounds and functions between the bounds that obey the fundamental physics.

The space of functions, $\mathcal{F}$, with ranges that span the manifold $\mathcal{Y}$ between the physical uncertainty bounds (PUBs) while respecting the constraints imposed on q_N by the fundamental physics (monotonicity, convexity, ...) is infinite dimensional. Clearly, the feasibility of our proposed methodology hinges on obtaining a sufficient number of sample functions from $\mathcal{F}$. We will always include the functions with ranges that are the bounds. Forward propagation of the set of sample functions, which we denote $\mathcal{F}_S$, will never yield the exact extrema of the QoI over $\mathcal{F}$. However, in practice, it is only necessary that propagation of $\mathcal{F}_S$ results in at least one point in each neighborhood of the extrema of the QoI. Our proposed uncertainty quantification methodology will constitute a practical means of obtaining upper bounds on the QoI, whereas, as we discuss below, parametric and model-selection methodologies provide, at best, lower bounds on the QoI, and are computationally expensive for simulations involving multiple physics categories.

Current research indicates that the generation of monotone, convex sample functions between the PUBs is a tractable problem. For instance, Stationary Random Process theory (SRP) is being used to generate such samples for the HE EOS physics process [24]. Monotonicity and convexity are generally required by the physics and therefore also apply to many other physics processes (e.g., cold shear modulus,

finite-T shear modulus, flow stress vs. plastic strain rate, ...), hence this SRP approach can be used to generate samples for many physics processes.

Three approaches are being developed to select a low-dimensional parameterized family of functions from $\mathcal{F}$; a subset of parameter values defines $\mathcal{F}_S$. Each of these approaches allows for the application of rigorous statistical and mathematical strategies (e.g., GPM, optimization techniques, ...).

The first and simpliest method, is to discretize the space between the bounds and consider only functions that run through discretized levels of points. This method has the clear disadvantage of adding strong constraints on $\mathcal{F}_S$, but it has the advantage of inducing a clear ordering on the functions in $\mathcal{F}_S$. We expect many of the physics processes being considered will be monotone with respect to this ordering and wish to confirm that hypothesis.

In the second method, which has been applied to the HE EOS, the function space between the PUBs is reduced to a two-parameter family of functions (this work, in addition to the SRP theory, can be found in [24]); most HE EOSs have more than two parameters. This is accomplished by considering two quantities of interest and taking their functional directional derivatives to determine, to first order, which directions the quantities of interest depend on. This method has the advantage of imposing no additional restrictions on $\mathcal{F}$, but has the disadvantage of requiring relevant quantities of interest for a given physics process; subject matter expertise is needed to identify these QoIs.

The third method is similar to the well-known Kennedy O'Hagan method [4] for accounting for model-form uncertainty (discussed in both [1] and [2]). This approach has the advantage of working for any physics process where at least one known model is interior to the bounds, but has the disadvantage of requiring additional restrictions on $\mathcal{F}_S$. It is certainly not as restrictive as the first method discussed and, by design, subject matter expertise can be used to justify these additional constraints.

There are generally multiple models (and corresponding sub-models) for a given physics process, each based on differing sets of approximations. Consequently, there is an uncertainty in the calculated engineering performance associated with the existence of a multiplet of models in a particular physics category, but this uncertainty is not taken into account by parametric methodologies.

Model selection methodologies entail switching out physics models to determine the uncertainty in calculated system performance. A model selection methodology accounts for all available models in a given physics category, of course excluding models that can be rejected as unreliable because they are based on poor approximations or erroneous assumptions, and in general the resulting uncertainty in calculated system performance exceeds that of parametric methodologies. However, as a specific physics phenomenon becomes better understood (theoretical advances and new experimental data) more models are developed, hence the model selection uncertainty on calculated system performance will increase unless data or theory can elimate an existing physics model. This is a clear indication that, like parametric methodologies, model selection methodologies generally provide only a lower bound on calculated system performance. In particular, when only one (or no) model(s) is (are) available in a physics category, any model selection methodology gives an uncertainty of zero. Therefore, model selection methodologies can result in extremely optimistic measures of the uncertainty in calculated system performance.

In Section 3.1, we will show that parametric and model selection methodologies generally fail to bound the physical process uncertainty. Unfortunately, the parameters of physics models are not designed to, and in fact generally do not, span the uncertainty (the model's fidelity for the physics process). We show that even for physics models and physics regimes where focused experiments are available, the physics model parameters are not designed to, and typically do not, bound the experimental uncertainty (which could, in this idealized circumstance, serve as a surrogate for the model fidelity uncertainty). Model parameter sets are often designed to distinguish between similar physical systems (e.g., to move between types of HE or metals), but not to bound the experimental or theoretical uncertainties. For this reason, many physics models simply have no parameters to vary and this lack of parameters has nothing to do with the fidelity of the given physics model. Moreover, it is exactly where the model fidelity uncertainty is high that the theorist does not provide parameters. For instance, Cu and U, which differ by an order of magnitude in their flow stresses, are distinguished by markedly different flow stress parameter sets, but it is not possible to vary the model parameters so that the flow stress variations coincide with the model fidelity uncertainty for either Cu or U. Also, when physics model parameters are varied to quantify uncertainty in a data rich regime these bounds can artificially expand/contract when the model is used to extrapolate to a regime where experimental data are unavailable.

The remainder of this paper is organized as follows. Section 2 describes five physics categories: plasma fusion reactions, material damage, neutronics, material strength, and HE. We provide a breakdown of each physics category into its individual physics processes. To model the physics category a physics

model for each of the processes is required. We limit our descriptions of individual physics models to the ones that will be used for illustrative purposes in Section 3. Section 3 discusses the limitations of parametric or model selection methodologies for determining the uncertainty in simulating engineered systems. In particular, we address why parametric methodologies are not applicable for addressing the uncertainty associated with using physics models to approximate physics processes, and the shortcomings of combined parametric and model selction methodologies. In Section 4 we discuss strategies for bounding our theoretical and experimental uncertainty. For illustration purposes, we discuss several approaches that either have, are, or could be taken to bound the physics for several different physics processess. We show that the bounds being developed are independent of any specific model or its parameters. The result is that for each physical process the uncertainty can be represented by a bounded functional space with strong physics constraints. Initial research on sampling from these functional spaces can be found in [24]. In Section 5 we summarize our conclusions. Appendix A elucidates the definition of a physics category.

No system performance simulations are shown in this paper.

2 Physics categories: five examples

In this Section we discuss five physics categories that will be used for illustrative purposes in the remainder of the paper. The five physics categories discussed are plasma fusion reactions, material damage, neutronics, material strength, and HE. We define a physics model to be the set of equations and associated parameters that describe an idealized physical system. Generally, it takes several physics models to model a specific physics category. Several of the physics categories are broken down into possible composite continuum-level physics models to give the reader an idea of the complexity of the individual categories as well as an appreciation for the number of models and sub-models associated with the given physics category. Specific models and sub-models are described to the extent needed to understand the rest of the paper.

In Section 2.1 we consider the plasma fusion reaction physics category. We focus on plasma stopping power, and describe the Li-Petrasso model. Section 2.2 concerns the material damage physics category. We briefly discuss two cumulative damage models, the Hancock-Mackenzie and Johnson-Cook models, as well as the TEPLA framework. We show how these models are coupled with melt temperature and flow stress degradation models to create possible composite continuum-level models for the damage physics category. Three models of flow stress degradation due to material damage are discussed: Cochran-Banner, Binary, and Linear. In Section 2.3 we discuss the neutronics physics category. An important aspect of neutronics – prompt fission neutron spectra – is used to illustrate several of the points in this paper. We discuss the Maxwellian, Watt, and Madland-Nix physics models for the PFNS physics process. The material strength physics category is the topic of Section 2.4. We limit ourselves to three flow stress (strength) models: Steinberg-Cochran-Guinan, Preston-Tonks-Wallace (PTW), and Johnson-Cook. We show how these models are coupled with melt temperature and shear modulus models to create possible composite continuum-level models for the strength category. Two models for the temperature- and pressure-dependent shear modulus, the Straub and Burakovsky-Greeff-Preston models are discussed. Finally, we consider HE physics category in Section 2.5. We discuss the Huygens construction (Lund) and Detonation Shock Dynamics (DSD) HE burn models. There are many possible routes for modeling HE detonation products; we limit our discussion to the Jones-Wilkins-Lee (JWL) model.

2.1 Physics category: plasma fusion reactions

The nuclear fusion reaction rate (number of fusions per unit volume per unit time) of a plasma is given by the expression

$$reaction\ rate = n_1\, n_2\, <\sigma\, v>, \tag{8}$$

where n_i is the number density of nuclear species i, σ is the energy-dependent reaction cross section, v is the relative velocity, and the average is weighted by the velocity distribution, e.g. a thermal distribution. The reaction cross section can be strongly energy dependent; for example, the D-T cross section varies by over three orders of magnitude from $0.002\,b$ to $5\,b$ as the center-of-mass energy varies by one order of magnitude from $10\,keV$ to $100\,keV$. In a numerical simulation involving plasma fusion reactions, the reactant densities, the electron and ion temperatures, and the pressure are related through the plasma EOS. As the fusion reaction products traverse the plasma they deposit their kinetic energies in the ions

and electrons of the plasma, and therefore slow down and heat the plasma. This energy deposition during charged particle transport is characterized by dE_b/dx, the energy transferred to plasma species b per unit distance travelled by the charged test/projectile particle. Finally, it is necessary in general to account for electron-ion thermal equilibration.

In Section 3 we illustrate an important point about parametric methodologies with the well-known Li-Petrasso model of plasma stopping power, i.e. dE/dx. In preparation for that example, we now provide some background material on stopping power and the model of Li and Petrasso.

The stopping power includes contributions from both short-distance, hard Coulomb collisions and long-distance, collective excitations of the plasma. The squared projectile-plasma coupling may be defined as

$$g^2 = \sum_b \beta_b^2 \left(\frac{e_p\, e_b}{4\,\pi}\right)^2 \kappa_b^2\,, \tag{9}$$

where the sum is over plasma species b, $\beta_b = 1/T_b$, e_p (e_b) is the projectile (species b) charge in rationalized cgs units, and $\kappa_b^2 = \beta_b e_b^2 n_b$, with n_b the number density of species b, is the squared Debye wavenumber of species b. The stopping power for weak coupling is of the generic form $dE/dx = B\,g^2\,\ln(C\,g^2) + \mathcal{O}(g^3)$. Brown, Preston, and Singleton (BPS) have evaluated both B and C by means of a novel application of dimensional continuation which combines the long- and short-distance physics encoded in the Lenard-Balescu and Boltzmann equations without invoking arbitrary cutoffs [15]. We emphasize that the result of BPS is not a model but rather the exact small-coupling limit. The strong-coupling regime can only be investigated by means of numerical simulations.

Many dE/dx models have been constructed [8, 9, 10, 11, 12, 13, 14], but here we make no attempt to provide an exhaustive discussion. Instead, we consider only the model of Li and Petrasso [12], which we use for illustrative purposes in Section 3. They evaluated the stopping power to leading order in the plasma coupling (B above) but could only estimate the constant C under the logarithm, which was computed exactly by BPS. A term involving a step function was added to correct for collective effects. Their model may be written as follows:

$$\begin{aligned}
\frac{dE_{LP}}{dx} &= \frac{e_p^2}{4\,\pi}\frac{1}{v_p^2}\sum_b \frac{\kappa_b^2}{\beta_b\, m_b}\left[-\frac{1}{2}\,G\left(\frac{1}{2}\beta_b m_b v_p^2\right)\,\ln\left(\kappa_D^2 B_b^2\right) + H\left(\frac{1}{2}\beta_b m_b v_p^2\right)\right]\,, \qquad (10)\\
G(y) &= \left[1 - \frac{m_b}{m_p}\,\frac{d}{dy}\right]\mu(y)\,,\\
H(y) &= \frac{m_b}{m_p}\left[1 + \frac{d}{dy}\right]\mu(y) + \theta(y-1)\,\ln\left(2e^{-\gamma}y^{1/2}\right)\,,\\
\mu(y) &= \frac{2}{\sqrt{\pi}}\int_0^y dx\, z^{1/2}\,\exp(-z)\,,\\
B_b^2 &= \left(\frac{\hbar}{2m_{pb}u_b}\right)^2 + \left(\frac{e_p\, e_b}{4\pi m_{pb} u_b^2}\right)^2\,, \quad u_b^2 = v_p^2 + \frac{2}{m_b}\,.
\end{aligned}$$

The subscript p refers to the projectile/test particle, $\kappa_D^2 = \sum_b \kappa_b^2$ is the total Debye wavenumber, m_{pb} is the reduced mass of the projectile and species b, and $\gamma = 0.577216\ldots$ is Euler's constant.

2.2 Physics category: material damage

The dynamic failure process in brittle and ductile metals is controlled, in general, by the strain rate, the stress state, the temperature, and the loading history. Since the 1960s, many dynamic failure models have been proposed. Here we focus on three models: the Hancock-MacKenzie [25] and Johnson-Cook [26] strain-to-fracture models, and the TEPLA framework [27]. The TEPLA framework integrates porosity growth with dynamic failure and requires the selection of a failure model, e.g. Hancock-Mackenzie or Johnson-Cook. These models are coupled with melt temperature and flow stress degradation models to create several possible composite continuum-level models for the damage physics category.

Cumulative damage is represented by a scalar field, D, which is zero in virgin material and equals 1 at failure. Note that D does not describe the actual microstructure evolution of the damage process, i.e. crack formation and propagation in brittle metals or void nucleation, growth, and link-up in ductile metals.

The one-parameter Hancock-MacKenzie (HM) model is

$$\frac{dD}{dt} = \frac{\dot{\epsilon}}{\epsilon_f} \tag{11}$$

where ϵ is the plastic strain rate and

$$\epsilon_f = \alpha \, \exp\left(\frac{3}{2}\frac{\bar{P}}{\sigma}\right) \tag{12}$$

is the fracture strain. In (12), σ is the flow stress and $\bar{P} = -Tr\left(\boldsymbol{\sigma}\right)/3$ is the mean compressive stress (pressure). The HM model is so simple it is tempting to view it as a statistical fit to data, but it is not. In fact, it is based on the result of Rice and Tracy for the growth rate of a spherical void in a perfectly plastic metal [28]. They found that the rate of change of the radius, R, is given by

$$\frac{\dot{R}}{R} = 0.28\,\dot{\epsilon} \, \exp\left(-\frac{3}{2}\frac{\bar{P}}{\sigma}\right) . \tag{13}$$

If it is assumed that the strain to fracture is inversely proportional to the growth rate, an assumption based on observation, and that no appreciable plastic flow occurs prior to void nucleation, then Eq. (12) follows. For metals where appreciable plastic flow does occur before nucleation, a constant term (pre-nucleation strain) could be added to the right hand side of Eq. (12), as pointed out by Hancock and Mackenzie [25].

Damage evolution in the five-parameter Johnson-Cook model is described by Eq.(11), but the fracture strain is a generalization of the Hancock-MacKenzie form (12) that includes strain rate and temperature dependencies:

$$\epsilon_f = \left[D_1 + D_2 \exp\left(-D_3\frac{\bar{P}}{\sigma}\right)\right]\left[1 + D_4 \, \ln\left(\frac{\dot{\epsilon}}{\dot{\epsilon}_0}\right)\right]\left(1 + D_5 T^*\right) . \tag{14}$$

Here $\dot{\epsilon}_0 = 1s^{-1}$ and T^* is the homologous temperature

$$T^* = \frac{T - T_{RT}}{T_m(\rho) - T_{RT}} \tag{15}$$

where $T_m(\rho)$ is the melting temperature at a given density, ρ and $T_{RT} = 298$K is room temperature. Note that T^* is a function of the melting temperature at the current density. In simulations, T_m is provided by another physics model. The dimensionless parameters D_1, D_2, D_4, and D_5 are positive, but $D_3 < 0$.

In the well-known TEPLA framework [27], which encompasses existing damage and strength models, the fracture condition is written

$$\left(\frac{\phi}{\phi_f}\right)^2 + \left(\frac{\epsilon}{\epsilon_f}\right)^2 = 1 , \tag{16}$$

where $\phi \in [0, 1]$ is the porosity and the critical (maximum) porosity, ϕ_f, is a material parameter. It follows from (16) that porosity decreases the strain at fracture from ϵ_f to

$$\hat{\epsilon}_f = \epsilon_f \left(1 - \frac{\phi^2}{\phi_f^2}\right)^{\frac{1}{2}} . \tag{17}$$

Figure 5 shows several examples of two basic types of composite damage models, those that involve only a fracture strain ϵ_f, and TEPLA models that incorporate porosity evolution. In either case, fracture/failure occurs instantaneously when the damage parameter, D, equals unity.

Figure 6 illustrates the interplay of the damage models in a simulation and includes flow stress degradation. In summary, the pressure-dependent melt temperature, T_m, is calculated and if $T < T_m$ the fracture strain and (if TEPLA) porosity are computed, and the scalar damage D is updated. The effective flow stress decreases with increasing material damage, i.e. with increasing D. The simplest flow stress degradation rule is the Binary rule [26] (no flow stress degradation until $D = 1$ at which point the flow stress is set equal to zero). A more realistic degradation model is the simple Linear model

$$\sigma = \sigma_0(1 - D) , \tag{18}$$

where σ_0 is the flow stress of undamaged material. Several other forms have been proposed, most notably that of Cochran and Banner

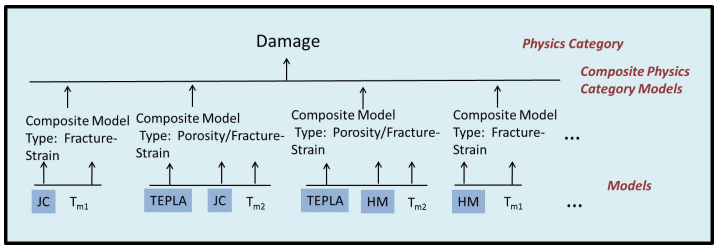

Figure 5: Composite material damage models are of two types, those that involve only a fracture strain, and TEPLA models.

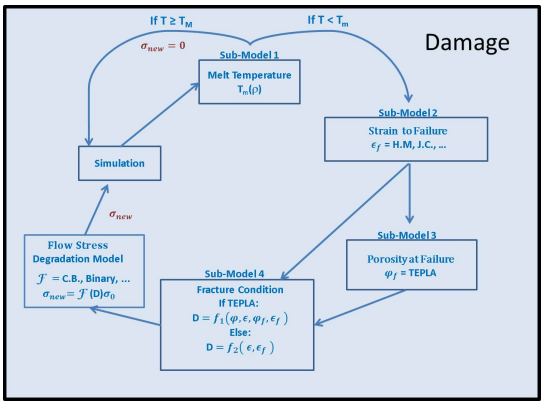

Figure 6: The interplay of damage models in a simulation.

$$\sigma = \sigma_0 \left(1 - \left(\frac{D}{D_0}\right)^{2/3}\right), \tag{19}$$

where σ_0 is the flow stress of undamaged material and $D_0 \in (0, 1]$ is the critical value of damage that corresponds to total fracture [29]. In general, a flow stress degradation model can be written in the form $\sigma = \sigma_0 \mathcal{F}(D)$.

2.3 Physics category: neutronics

Neutronics calculations yield the distribution of neutrons in position, direction, and energy as a function of time. Neutronics requires a composite continuum-level model that includes physics models for total cross sections, fission source, and scattering. Each of these models may be a composite model itself. To illustrate this, in Figure 7 the fission source model is broken down into the four required physics models: flux, fission cross section, nubar, and prompt fission neutron spectra (PFNS). Our focus here is on PFNS, i.e. the probability distribution in energy of neutrons emitted within about 10^{-14} s of nuclear fission rather than milliseconds to minutes later as a result of (usually) beta decay. We discuss three PFNS models in this paper: Madland/Nix, Maxwellian, and Watt; see Figure 5.

2.3.1 PFNS Models

Madland and Nix [5] identify the PFNS with the mean of the spectra for the light (L) and heavy (H) fission fragments. Assuming an energy-independent cross section for the inverse process of compound nucleus formation, they obtain the three-parameter laboratory spectrum

$$\begin{aligned} N(E) &= \frac{1}{2}\left[N(E, E_f^L) + N(E, E_f^H)\right], \\ N(E, E_f) &= \frac{1}{3\sqrt{E_f\, T_m}}\left[u_2^{3/2}\, E_1(u_2) - u_1^{3/2}\, E_1(u_1) + \gamma(\frac{3}{2}, u_2) - \gamma(\frac{3}{2}, u_1)\right], \\ u_1 &= (\sqrt{E} - \sqrt{E_f})^2/T_m, \quad u_2 = (\sqrt{E} + \sqrt{E_f})^2/T_m\,, \end{aligned} \tag{20}$$

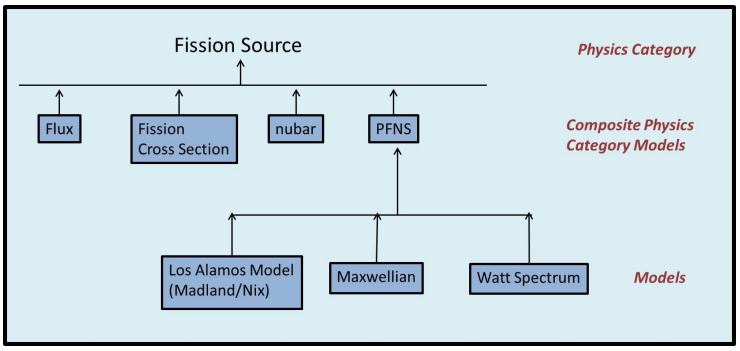

Figure 7: The neutronics category. It is shown that a fission source model is comprised of flux, cross section, nubar, and PFNS models.

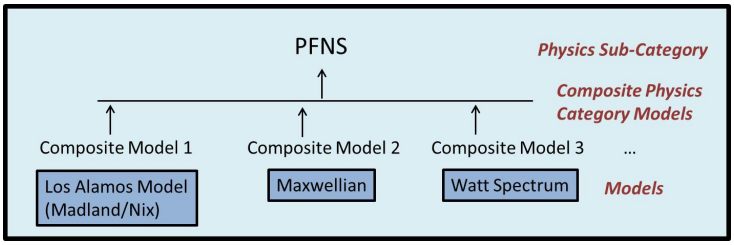

Figure 8: PFNS models

where

$$E_1(x) = -Ei(-x) = \int_x^\infty dt\, e^{-t}/t \tag{21}$$

is the exponential integral function and

$$\gamma(a,x) = \int_0^x dt\, t^{a-1}\, e^{-t} \tag{22}$$

is the incomplete gamma function. The mean kinetic energies per nucleon of the light and heavy fragments are given by

$$E_f^L = \frac{A_H}{A_L}\frac{< E_f^{tot} >}{A}, \quad E_f^H = \frac{A_L}{A_H}\frac{< E_f^{tot} >}{A}, \tag{23}$$

where A is the mass number of the fissioning nucleus, $A_{L,H}$ are the average mass numbers of the light and heavy fragments, and $< E_f^{tot} >$ is the average total fission fragment kinetic energy; A_L, A_H, and $< E_f^{tot} >$ are obtained from experiment. The mean laboratory neutron energy for this spectrum is given by

$$< E >= \frac{1}{2}\,(E_f^L + E_f^H) + \frac{4}{3}\,T_m\,. \tag{24}$$

The quantity T_m appearing in (20) and (24) is the maximum fission fragment residual nuclear temperature. Madland and Nix use the following expression for the residual temperature:

$$T_m = \left\{\frac{\epsilon\ < E^* >}{A}\right\}^{\frac{1}{2}}\ ; \tag{25}$$

$< E^* >$ is the total fission fragment excitation energy and $\epsilon = 11MeV$. However, T_m may be treated as a model parameter with an associated uncertainty.

The most notable predecessor of the Madland-Nix model is the two-parameter Watt model [6] [2]

$$N(E) = const \times e^{-E/Q}\, \sinh\left[2Q^{-1}(E\,E_f)^{1/2}\right]\,. \tag{26}$$

[2]In fact, this model was not initially proposed by Watt. In his paper, Watt states: "Several early reports on the fission spectrum mention this formula but none give the originator. It seems likely that it was derived by several investigators and spread by private communication."

By requiring that the mean energy is given by (24) the normalized Watt spectrum assumes the form [5]

$$N(E) = \frac{\exp(-E_f/T_W)}{\sqrt{\pi\, E_f\, T_W}} \sinh\left[2\,(E\,E_f)^{1/2}/T_W\right] , \tag{27}$$

where $T_W = 8\,T_m/9$ is the effective Watt temperature.

Another early PFNS model is the Maxwellian [7]

$$N(E) = \frac{2\sqrt{E}\,\exp(-E/T_M)}{\sqrt{\pi}\,T_M^{3/2}} , \tag{28}$$

where T_M, the effective Maxwellian temperature, is the only model parameter. However, if we again require that the mean energy be given by (24), the effective temperature is $T_M = (E_f^L + E_f^H)/3 + 8\,T_m/9$ [5].

2.4 Physics category: material strength

This category is defined by the principal variable returned to a code by a material strength model – the flow stress, σ – which is often referred to as the strength. The flow stress is the averaged shear stress (more precisely, $\sigma = \sqrt{3\,J_2}$, where $J_2 = s_{ij}s_{ji}/2$ is the second rotational invariant of the stress deviator tensor $s_{ij} = \sigma_{ij} - P\delta_{ij}$) required to induce plastic (inelastic, unrecoverable) deformation of a solid. It is a nonlinear function of the plastic strain rate, $\dot{\epsilon}$, the plastic strain, ϵ, and the material density and temperature. Composite strength models involve three physics models. One is the basic plastic constitutive relation. A model of the density- and temperature-dependent shear modulus, $G(\rho, T)$, is needed because the flow stress in several of the constitutive relations is scaled by G. Finally, a model of the density-dependent melt temperature is needed both to calculate the constitutive relations for flow stress and because the flow stress is zero when the material melts. The relationships between these models are diagrammed in Figure 9.

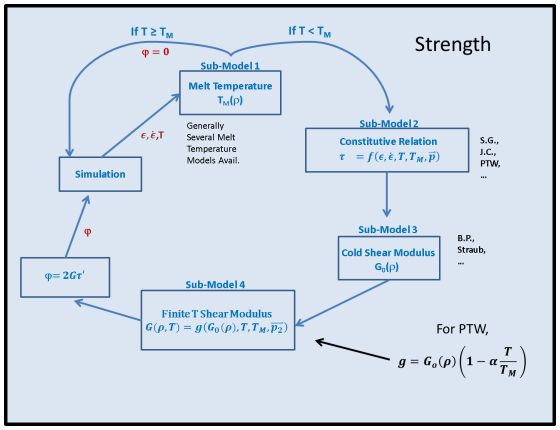

Figure 9: The material strength category includes models for the plastic constitutive behavior, the density- and temperature-dependent shear modulus, and the density-dependent melting temperature.

Many material strength models have been developed, most notably the Hoge-Mukherjee [30], Steinberg-Cochran-Guinan (SCG) [31], Johnson-Cook [32], Zerilli-Armstrong [33], Mechanical Threshold Stress (MTS) [34], Steinberg-Lund [35], Preston-Tonks-Wallace (PTW) [20], and Langer-Bouchbinder-Lookman [36] models. We now consider the Johnson-Cook, PTW, and SCG models to illustrate the basic features of a material strength model.

The five-parameter Johnson-Cook model is

$$\sigma = (A + B\,\epsilon^n)\left[1 + C\,\ln\left(\frac{\dot{\epsilon}}{\dot{\epsilon}_0}\right)\right](1 - T^{*m}) , \tag{29}$$

where $\dot{\epsilon}_0 = 1s^{-1}$ and T^* is the homologous temperature defined by Eq. (15). When the strength physics category is simulated the melt temperature, T_m, is provided by a separate physics model. The three factors in (29) account for work hardening (strength increases with strain), strain rate dependence, and thermal softening.

The PTW model is applicable at strain rates from $10^{-4}s^{-1}$ to about $10^{12}s^{-1}$. It involves eleven dimensionless parameters, all of which have a clear physical interpretation. The model interpolates between the low-rate thermally-activated dislocation glide regime and the very high rate strong-shock limit, thus it is least reliable at intermediate strain rates, generally 10^5s^{-1} to around 10^7s^{-1}. All stresses in the model are scaled by the density- and temperature-dependent shear modulus, $G(\rho, T)$; scaled stresses are denoted with a caret. The scaled saturation (large strain) and yield (zero strain) stresses ($\tau = \sigma/2$) are

$$\hat{\tau}_s = s_0 - (s_0 - s_\infty)\,\mathrm{erf}\left[\kappa\hat{T}\ln\left(\gamma\dot{\xi}/\dot{\epsilon}\right)\right], \tag{30}$$

$$\hat{\tau}_y = y_0 - (y_0 - y_\infty)\,\mathrm{erf}\left[\kappa\hat{T}\ln\left(\gamma\dot{\xi}/\dot{\epsilon}\right)\right]. \tag{31}$$

In these expressions, $\hat{T} = T/T_m(\rho)$ is density and temperature dependent, and $\dot{\xi}$ is the reciprocal of the time required for a transverse sound wave to cross an atom. Work hardening is described by a modification of Voce [37] behavior

$$\frac{d\hat{\tau}}{d\epsilon} = \theta\,\frac{\exp\left[p\ \frac{\hat{\tau}_s-\hat{\tau}}{s_0-\hat{\tau}_y}\ \right]-1}{\exp\left[p\,\frac{\hat{\tau}_s-\hat{\tau}_y}{s_0-\hat{\tau}_y}\ \right]-1}, \tag{32}$$

which integrates to

$$\begin{aligned}\hat{\tau} &= \hat{\tau}_s + \frac{1}{p}\,(s_0-\hat{\tau}_y)\,\ln\left[1-\left[1-\exp\left(-p\,\frac{\hat{\tau}_s-\hat{\tau}_y}{s_0-\hat{\tau}_y}\right)\right]\right.\\ &\times \left.\exp\left\{-\frac{p\,\theta\,\epsilon}{(s_0-\hat{\tau}_y)\,\left[\exp\left(p\,(\hat{\tau}_s-\hat{\tau}_y)/(s_0-\hat{\tau}_y)\right)-1\right]}\right\}\right].\end{aligned} \tag{33}$$

The Steinberg-Cochran-Guinan rate-independent flow stress is given by

$$Y(\epsilon, P, T) = \min\left[Y_0\ \left[1+\beta\,(\epsilon+\epsilon_i)\right]^n, Y_{max}\right]\left\{1+\frac{G'_P}{G_0}\,\frac{P}{\eta^{1/3}}+\frac{G'_T}{G_0}\,(T-T_0)\right\}. \tag{34}$$

In Eq. (34), ϵ_i is the initial plastic strain (usually zero), G_0 is the shear modulus at the reference temperature T_0 and zero pressure, η is the material compression, and G'_P (G'_T) is the pressure (temperature) derivative of the shear modulus at $P = 0$ ($T = T_0$).

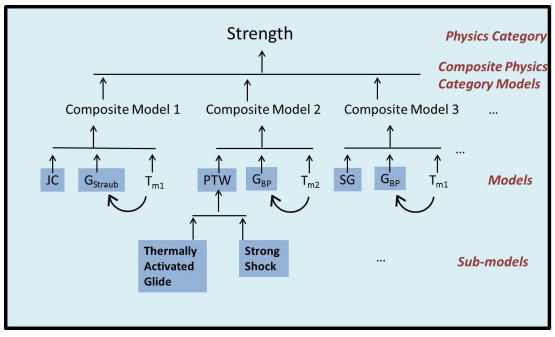

Figure 10: Composite models in the material strength category.

We now discuss two models for the cold (T=0K) shear modulus: Burakovsky-Greeff-Preston (BGP) [22] and Straub [21] and one for the temperature dependent shear modulus (Finite T): Preston and Wallace [38]. In the BGP model the density dependence of the shear modulus at zero temperature is

$$G_0(\rho) = G_0(\rho_0)\left(\frac{\rho}{\rho_0}\right)^{4/3}\exp\left\{6\gamma_1\left(\frac{1}{\rho_0^{1/3}}-\frac{1}{\rho^{1/3}}\right)+\frac{2\gamma_2}{q}\left(\frac{1}{\rho_0^q}-\frac{1}{\rho^q}\right)\right\}. \tag{35}$$

Here $G_0(\rho) \equiv G(\rho, T = 0)$, ρ_0 is a reference density, generally the density at zero pressure and temperature, and γ_1, γ_2, and q are dimensionless parameters that are determined from data.

The roles of the plastic constitutive relation, a shear modulus model, and a model for $T_m(\rho)$ in the strength category are diagrammed in Figure 10.

The density dependence of the shear modulus at constant temperature was modeled by Straub as

$$G(\rho) = G_0 + g_1 \frac{a(\rho) - a(\rho_0)}{a(\rho)^2} \exp\left\{-g_2 \left[a(\rho) - a(\rho_0)\right]\right\} , \tag{36}$$

where

$$a(\rho) = \left(\frac{11.206\,\xi\,A}{\rho}\right)^{1/3} , \tag{37}$$

is the lattice constant in units of the Bohr radius. The quantity ξ is the number of atoms per unit cell, A is the atomic weight, ρ_0 is a reference density, $G_0 = G(\rho_0)$, and g_1 and g_2 are parameters.

The temperature dependence of G is approximately represented by a simple T-dependent factor [38]

$$G(\rho, T) = G_0(\rho) \left[1 - \alpha \frac{T}{T_m(\rho)}\right] . \tag{38}$$

A model for the density-dependent melt temperature, $T_m(\rho)$, is needed to (1) determine if the material is solid or liquid, and (2) to calculate the T dependence if Eq.(38) is used.

2.5 Physics category: HE

This category concerns high explosive (HE) burn models and the equations of state (EOS) of the detonation products.

Many wave-propagation codes a Huygens construction (Lund), to propagate HE detonation waves through the computational mesh. This can provide a good estimate of arrival times in HE geometries for which the propagation is not dominated by diffraction effects, and in regions sufficiently far removed from the initiation site. Huygens construction cannot describe corner turning or dead (shadow) zones, nor can it be applied where there are significant reaction zone effects. In such cases, the Detonation Shock Dynamics (DSD) model of Bdzil and Stewart [39], which accounts for the dependence of the propagation velocity on the burn front curvature, provides a superior description of the burn. The DSD equations follow from a small curvature (reaction zone length << radius of curvature of the burn front) expansion of the reactive Euler equations for inviscid flow.

An HE EOS relates the pressure to the internal energy density and the specific volume of the detonation products. Shock-wave propagation through the detonation products is governed by the EOS. Several

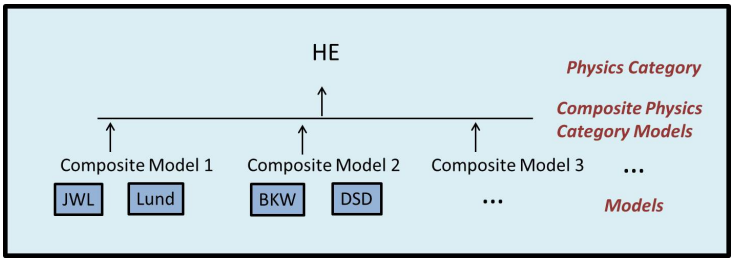

Figure 11: Composite Models in HE Category

detonation product EOSs have been constructed, in particular the BKW (Becker-Kistiakowski-Wilson) [40] and JWL (Jones-Wilkins-Lee) [41] equations of state; the JWL form is the most widely used EOS in the explosives community. The pressure, P, is a function of the internal energy density, ε, and the dimensionless specific volume, $v = V/V_0$. The energy density on the principal isentrope is

$$\varepsilon_s = \frac{A}{R_1} e^{-R_1 v} + \frac{B}{R_2} e^{-R_2 v} + \frac{C}{\omega} v^{-\omega} ; \tag{39}$$

the corresponding pressure is $P_s = -\partial\varepsilon_s/\partial v$. The EOS off the principal isentrope is of the Mie-Gruneisen form with $\gamma = \omega$:

$$P = A\left(1 - \frac{\omega}{R_1\, v}\right) e^{-R_1\, v} + B\left(1 - \frac{\omega}{R_2\, v}\right) e^{-R_2\, v} + \frac{\omega\, \varepsilon}{v}\,. \tag{40}$$

The parameters A, B, and C have the dimensions of pressure, while R_1, R_2, and ω are dimensionless. The three terms in (40) dominate the EOS at progressively lower pressures and at higher specific volumes. The first term controls the EOS at pressures near P_{CJ} and higher; P_{CJ} is the Chapman-Jouguet pressure, the pressure at the back of the reaction zone. The cylinder tests used to determine the model parameters are limited to $P < P_{CJ}$, hence the uncertainties in A and R_1 are relatively high, i.e. the JWL EOS is least reliable at pressures above P_{CJ}.

3 Why are we not using parametric or model selection methodologies to bound the uncertainty?

In Section 4 we will introduce a new methodology for determing bounds on the uncertainties in simulating engineered systems due to limited fidelity in physics models. In this Section, we explain why such a new methodology is needed. In particular, we show that parametric and/or model selection methodologies are not sufficient for determining the uncertainty associated with our ability to model a physical process.

In Section 3.1 we show that parametric methodologies cannot account for the uncertainty associated with using physics models to approximate physics processess. Finally, in Section 3.2 we consider combined parametric and model selection methodologies, and show that they are characterized by unexplored areas of uncertainty and we will show provide only lower bounds on the uncertainty.

3.1 Parametric methodologies for uncertainty quantification are not applicable to physics models

Parametric methodologies can be used to determine the probability of a set of parameters given the model and data, and therefore can provide a means of calibration to data. However, for these methodologies to be appropriate for determining the uncertainty in calculated system performance, it must be possible to vary the parameters in a way that represents the uncertainty associated with the model's fidelity. In this Section, we show that since physics models are, by definition, approximations designed to model average (mean) behavior given a set of approximations, parametric methodologies do not, in general, meet the above criteria. The fundamental assumption underpinning the application of a parametric methodology to quantify the uncertainty in simulating an engineered system is that the physics model parameters can be varied to exactly cover, or span, the uncertainty in the experimental, or possibly numerical, data, or ranges of uncertainty obtained by an understanding of the approximations and assumptions that governed the development of the physics model. Of course, if the physics model is a physics law then the functional form of the model in conjuction with data can be used to find the uncertainty on the parameters, and exactly covering the uncertainty is not required. For the sake of brevity, in the definitions below, all of these uncertainties will be referred to as data. We now provide a rather formal, but brief, discussion of the conditions necessary for the application of a parametric methodology.

We begin by reiterating some of the definitions from the Introduction. Let $\{q_i\}$, $i = 1, \ldots, N$, be a set of physical quantities, one of which, say q_N, is approximated, $\hat{q}_N$, with a physics model as a function of $q_1, \ldots, q_{N-1}$, which are coordinates of R^{N-1}, and a set of parameters, $\{p_j\}$, $j = 1, \ldots, M$, which are likewise coordinates in R^M. A physics model may be expressed as

$$\hat{q}_N = \mathcal{M}\left(\{q_1, \ldots, q_{N-1}\}, \{p_j\}, \{m_k\}\right), \tag{41}$$

where the $\{m_k\}$ are values that must be obtained from other physics models. A physics model is constructed using some combination of experimental and simulation data on q_N, and approximate theoretical representations of the dependence of q_N on $q_1, \ldots, q_{N-1}$, each over limited ranges of the $q_1, \ldots, q_{N-1}$. Therefore, the model is applicable only on a submanifold of R^{N-1} which will be called $\mathcal{Q}$. The q_N data have associated error bars, and in regimes where there are no data, q_N can be bounded on the basis of theoretical understanding of the physics process. The bounds on q_N are assumed (convenient, but not necessary) to be symmetric about a central value, $\bar{q}_N(q_1, \ldots, q_{N-1})$; the error is denoted $\delta q_N(q_1, \ldots, q_{N-1})$.

The N-dimensional manifold $\mathcal{Y}$ is defined as

$$\mathcal{Y} = \{(q_1, \ldots, q_N) \,|\, \bar{q}_N - \delta q < q_N < \bar{q}_N + \delta q, (q_1, \ldots, q_{N-1}) \in \mathcal{Q}\} \;, \tag{42}$$

that is, $\mathcal{Y}$ is the set of all data bounded by the error bars. We define $\hat{\mathcal{Y}}$ to be the set of all parametric variations that obey the bounds in Eq. 42.

Consider the determination of $\hat{\mathcal{Y}}$ for a physics law, $\mathcal{L}$, which by definition can be derived from established physics without making any significant approximations. For the sake of simplicity, we assume that all experimental uncertainty has been removed. Then, in general, there exists a connected domain $\mathcal{P}$ in R^M such that the continuous map

$$\mathcal{L} : \mathcal{Q} \times \mathcal{P} \rightarrow \mathcal{Y} \tag{43}$$

is surjective (onto), i.e., for each $y \in \mathcal{Y}$ there exists at least one $x \in \mathcal{Q} \times \mathcal{P}$ such that $y = \mathcal{L}(x)$. The direct product $\mathcal{Q} \times \mathcal{P}$ is the covering space of $\mathcal{Y}$, thus $\hat{\mathcal{Y}} = \mathcal{Y}$. In other words, over the domain $\mathcal{P}$ of parametric variations, i.e. the prior, the modeled q_N exactly covers, no more and no less, the manifold $\mathcal{Y}$. If the physics law $\mathcal{L}$, as a map into the data/theory uncertainty, were not surjective then in calculating the uncertainty in a Quantity of Interest (QoI) we would overestimate or underestimate the uncertainty in q_N in at least one regime (region in the $q_1 - \ldots - q_{N-1}$ plane). Moreover, if we further assume that the bounds on q_N were derived from a set of distributions, then these distributions and the functional form of the physics law, $\mathcal{L}$, can be used to find a manifold $\hat{\mathcal{X}} \subseteq \hat{\mathcal{Y}} \subseteq \mathcal{Y}$ that represents the uncertainty in the parameters of $\mathcal{L}$ given the data. Even if $\hat{\mathcal{Y}} \neq \mathcal{Y}$, in general, $\hat{\mathcal{X}}$ is a reasonable approximation of the uncertainty. This is because a physics law is known and the uncertainty is how well data (or fundamental physics) can determine the parameters. We note here that there are statistically rigorous methodologies for determining $\hat{\mathcal{X}}$ that account for experimental uncertainties.

Now consider a true physics model rather than a physics law, which we rarely if ever have in practice. Physics models are approximations of physics processes. Using the functional form of a physics model to reduce the uncertainty results in potentially reducing the already lower bound, $\hat{\mathcal{Y}}$, on the uncertainty (when $\hat{\mathcal{Y}} \subseteq \mathcal{Y}$, right side of Figure 3) to $\hat{\mathcal{X}} \subseteq \hat{\mathcal{Y}}$, and when $\hat{\mathcal{Y}} = \emptyset$ the manifold $\hat{\mathcal{X}}$ is not even contained within the bounds, $\hat{\mathcal{X}} \not\subseteq \mathcal{Y}$ (Figure 4).

An obvious question is: Are the examples in the Introduction outliers? Can the parameters of a physics *model*, in general, be varied so that the uncertainty in the data is exactly covered, that is, can we always find a prior $\mathcal{P}$ such that $\mathcal{Q} \times \mathcal{P}$ is the covering space of $\mathcal{Y}$? The short answer is an emphatic "no" – this is not possible, even in principle. Do not miss our point: parametric methodologies for uncertainty quantification are not reasonable techniques for quantifying the uncertainty associated with our ability to *model* a physics process.

Before expounding on the reasons that parametric methodologies break down for physics models, we first show, by example, that the above criteria necessary for the application of a parametric methodology can be satisfied.

The performance of inertial confinement fusion (ICF) capsules depends on the rate at which the electrons and ions in a high-temperature plasma achieve thermal equilibrium. The rate of energy density transfer from the electrons (e) to ion species i can be written

$$\frac{d\mathcal{E}_{ei}}{dt} = -\mathcal{C}_{ei} \left(T_e - T_i\right), \tag{44}$$

where T_e and T_i are the instantaneous electron and ion temperatures, and $\mathcal{C}_{ei}$ has the dimensions $volume^{-1} time^{-1}$. A physicist constructs a multi-parameter model for $\mathcal{C}_{ei}$ which is implemented in the code used for system simulations. For the simplest case of hydrogen plasmas, the model assumes the form

$$\mathcal{C}_{ei} = c_1 \frac{n^2}{T_e^{3/2}} \ln\left(c_2 \frac{T_e^2}{n}\right) \tag{45}$$

where n is the electron or proton number density, and $c_{1,2}$ are parameters. An experimental effort is launched to acquire $\mathcal{C}_{ei}$ data over broad ranges of n and T_e. The experimenters, who are very talented, introduce no systematic uncertainties into the data. A parametric analysis is then undertaken and, as expected by the analysts, c_1 and c_2 can be varied around central values so as to exactly cover the uncertainty in the data, which are distributed around central values with an error that varies with n and T_e. In terms of our above notation, $c_{1,2}$ are in $\mathcal{P}$, $\mathcal{Q}$ is the experimental range in n and T_e, and $\mathcal{Y}$ is $\mathcal{C}_{ei} \pm$ error bars over n and T_e. It is confirmed that a parametric methodology is applicable: $\mathcal{Q} \times \mathcal{P}$ is the

covering space of $\mathcal{Y}$. At this point the modeler admits that she had derived Eq. (45) from fundamental theory, and wished to have her laborious calculations (which nevertheless led to a simple result) verified experimentally; she knew that $\mathcal{Q} \times \mathcal{P}$ would not cover $\mathcal{Y}$ if she had made a mistake. She also confirmed that the mean parameter values were in excellent agreement with the expressions she had derived for c_1 and c_2 in terms of fundamental physical quantities:

$$c_1 = \frac{e^4}{4\pi} \frac{1}{m_p} \sqrt{\frac{m_e}{2\pi}}, \quad c_2 = \frac{8}{\exp(\gamma + 1)} \frac{m_e}{e^2 \hbar^2}; \tag{46}$$

$\gamma = 0.5772\ldots$ is Euler's constant. The main message here is that Eq. (45) is not a physics model at all, but rather a relation obtained from fundamental theory [15], and the constants $c_{1,2}$ are not really physics model parameters but are combinations of fundamental quantities. It is generally only in such cases, cases where the "model" is perfect, that $\mathcal{Q} \times \mathcal{P}$ is the covering space of $\mathcal{Y}$ and a parametric uncertainty analysis is applicable. However, for fundamental relations such as Eq. (45) a parametric analysis is superfluous unless there are large uncertainties in the fundamental physical quantities underlying its "parameters." For example, an exact result might be expressed in terms of a nuclear cross section at a particular energy, but that cross section is not well known. On the other hand, for true physics models, which by definition involve assumptions and approximations and are therefore not fundamental relations, a parametric domain $\mathcal{P}$ (prior) for which $\mathcal{Q} \times \mathcal{P}$ is the covering space of $\mathcal{Y}$ does not exist: parametric methodologies cannot be meaningfully applied to physics models. Physics models are not probabilistic models with parameters representing our lack of knowledge so parametric methodologies will, in general, fail at providing the correct or even useful uncertainty.

In the remainder of this Section we provide many examples to illustrate that parametric variations in physics models cannot cover the uncertainties. There are several reasons, each addressed in the following four sub-sections, why this is not possible. In summary: (1) Some models have no (are almost no) parameters; (2) Approximations and assumptions are made to minimize model complexity, but the parameters introduced with the assumptions and approximations cannot, in general, be varied to span the experimental uncertainties; (3) There are often no parameters for physical regimes where there are no experimental or numerical data, i.e. there are no parameters to use to attempt to cover uncertainty in regimes without data; (4) Model parameters are often designed to capture mean behavior in a physical system, but such parameters cannot, in general, cover the experimental uncertainties.

3.1.1 Some models have no (or almost no) parameters

The Lund programmed burn model has one parameter that represents the HE velocity. This parameter can only change the burn front speed and is obtained experimentally with very small uncertainty ($< 1/2\%$) [16]. The one-parameter Lund programmed burn model is known to be quite accurate for low-curvature detonation wave fronts, but cannot accurately represent burn in systems where diffraction, corner turning, dead zones, or reaction zone effects are important. Even for such cases, a parametric methodology for uncertainty quantification would associate zero uncertainty with the Lund HE burn model. Application of the same methodology using a higher fidelity model, say the DSD HE burn model with 17 parameters, is bound to yield a larger uncertainty (since the HE velocity is one of the parameters the other 16 parameters need only result in changing the QoI by greater than zero).

One of the more successful models of plasma stopping power, the Li-Petrasso model described in Section 2.1, has no parameters (note that fundamental values such as electron mass are not parametric values that can be varied, they are constants). Therefore, $\hat{\mathcal{X}} = \hat{\mathcal{Y}} = \emptyset$. In Figure 12 we compare this model to the results of MD simulations of a point particle with charge $e_p = -10e$ traversing an electron gas [17]. Since it has no parameters, the model cannot span the uncertainties in the numerical data at low velocities, and a parametric methodology cannot be applied. However, when using this physics model in a simulation of an engineering system where the system is expected to spend some time at lower energies, it is exactly the impact of the low-fidelity of the Li-Petrasso model at lower energies on the QoI that one wants to quantify. There are simply **no** parameters that can be varied to quantify the impact of this approximation.

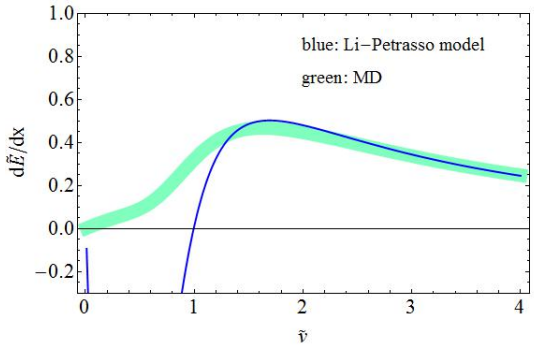

Figure 12: Comparison of the Li-Petrasso model (blue curve) to the results of MD simulations (green band) of a particle with charge $-10e$ moving through an electron gas. The stopping power and particle velocity are scaled, i.e. dimensionless (see [17] for details). The electron density is $1.03 \times 10^{20} cm^{-3}$ and $\Gamma = (e^2/4\pi T)(4\pi n_e/3)^{1/3} = 1$. The width of the green band indicates the approximate uncertainty in the numerical (MD) data.

Next consider the prompt fission neutron spectrum (PFNS) physics process from Section 2.3. The prompt fission neutron spectrum is the number of neutrons as a function of energy. This is known to be a near Maxwellian relation. Therefore, the simplest and probably most widely used PFNS model is a Maxwellian. In Figure 13[3], the PFNS data is normalized to a Maxwellian. For low energies, using a Maxwellian can be a very reasonable, Occam's razor approach. However, when using this physics model in a simulation of an engineering system where the system is expected to spend some time at higher energies, it is exactly the impact of the low-fidelity of the Maxwellian model at higher energies on the QoI that one wants to quantify. It can be seen in Figure 13 that variation of the only model parameter cannot be varied to quantify the impact of this approximation. In particular, $\hat{\mathcal{Y}} = \emptyset$ and $\hat{\mathcal{X}} \not\subseteq \mathcal{Y}$.

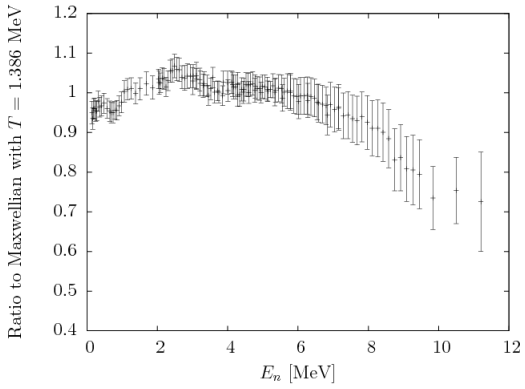

Figure 13: Prompt Fission Neutron Spectrum data normalized to a Maxwellian

The Binary [26] and Linear flow stress degradation models discussed in Section 2.1 are other examples of physics models with no parameters to vary. In this Section, we have provided five examples of physics models that simply have no (or almost no) parameters to vary. We could continue to provide examples, however, what we wish to convey is that parameters (and the number of parameters) in physics models have nothing to do with physics model's fidelity for the physics process. Therefore, they are not related to the uncertainty associated with the physics model's fidelity for modeling any given engineered system. For this reason, we move on to discussions of models with parameters.

[3]PFNS images provided by Sky Sjue, LANS.

3.1.2 Model approximations and assumptions

These fall into two basic groups, those that involve the use of functional forms that approximate the physics and those that eliminate the dependence of q_N on a subset of the q_i. In either case, it is generic that parametric variations cannot cover the uncertainties in the data.

Functional forms that approximate the physics
Almost all physics models rely on functional forms that approximate the physics. Often several functional forms are combined, each representing different regimes, length/time scales etc. Most of these functional forms have a physical meaning that the theoretician is using to approximate the physics. For instance, the Arrhenius equation is used in the development of the PTW flow stress model. It is an approximation of the true physics for which a fundamental physics law is not known. The Hancock-Mackenzie model is based on a functional form that is a theoretical approximation (a spherical void in a perfectly plastic metal) derived in [28]. In this Section, we chose to illustrate our points with three physics models from the literature where the approximations and assumptions that went into the model development are easy to articulate and, moreover, the models are for physics processes in regimes where data are available. Even for these simple models in these ideal data rich environments, parametric methodologies cannot account for the model fidelity uncertainty. The first is the example just discussed in Section 3.2.1. The approximation of the Maxwellian model, is simply that the PFNS is a Maxwell-Boltzmann distribution. Normalizing the data to a Maxwellian clearly indicates otherwise. The one parameter in the Maxwellian model cannot account for this approximation.

Consider the Preston-Wallace (PW) finite-temperature shear modulus model [38]. Recall, from Section 2.3, that this model is used in conjunction with the PTW flow stress (strength) model. Therefore, any uncertainty introduced by this model should be taken into account in an uncertainty quantification study that involves PTW. Simmons and Wang ([42]) provide data on the upper and lower bounds (Hashin-Shtrikman) on $G(P = 0, T)$, where P is pressure and T is temperature. Equation 1 of [38] can be used to convert the data from $P = 0$ to nominal density, ρ_0. The average behavior of the shear modulus as a function of temperature at nominal density, $G(\rho = \rho_0, T)$, can be obtained by taking the mean of the bounds. These mean values are shown in green for uranium and copper in Figure 14. The PW model is

$$G(\rho, T) = G(\rho, 0)\left(1 - \alpha \frac{T}{T_m(\rho)}\right). \tag{47}$$

The values of $G(\rho, 0)$ and $T_m(\rho)$ come from other models (e.g., [21], [22]). In Figure 14, the PW model is plotted in blue. The one-parameter PW model is a linear approximation to the mean of the nominal density bounds, where the parameter α is provided to differentiate between metals. An assumption of the model is that this near-linear relation holds for higher pressures.[4] This is a reasonable assumption because: (1) the linear approximation holds for all metals and alloys for which we have data, and since these metals have very different electronic structures, it is evident that the approximate linearity is insensitive to the electronic structure; (2) as P increases, the electronic structure changes, but the linear approximation is still expected to hold because of its insensitivity to the electronic structure. There are no parameters to account for this assumption or to improve on the linear approximation.

Now assume we are modeling G at nominal density. In Figure 15, we repeat the previous plot for U but add the Hashin-Shtrikman bounds from Simmons and Wang. We note that these are strict bounds – there is no statistical distribution in the value of G at a given temperature.

[4]The authors are carrying out quantum MD calculations to quantify the uncertainty introduced by this assumption.

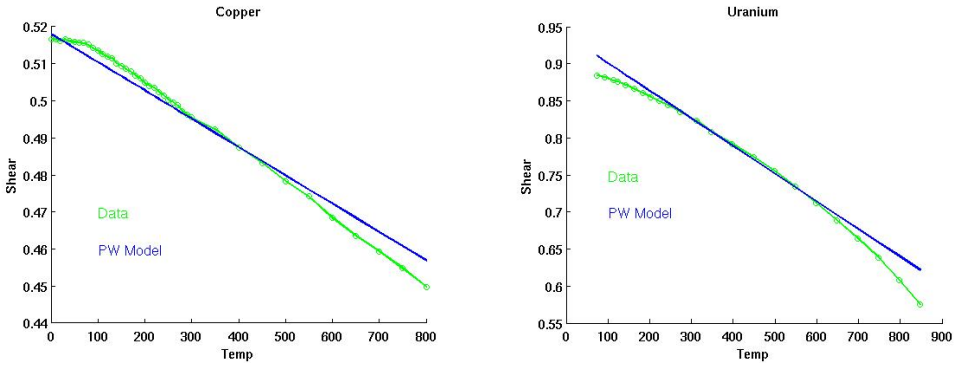

Figure 14: Comparison of the PW model of the shear modulus to $P = 0$ data on Cu and U.

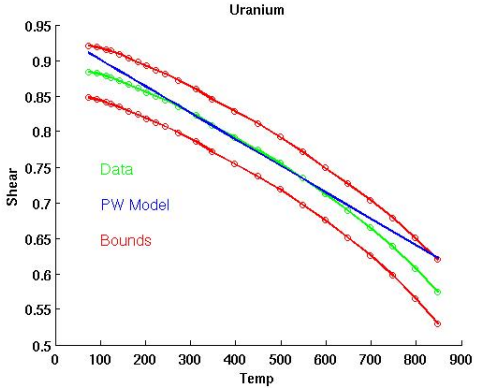

Figure 15: Uranium shear modulus versus temperature at $P = 0$; the data terminate at $0.6\,T_m$. The red curves are the Hashin-Shtrikman bounds, the green is the average of the bounds, and the blue straight line is the PW model.

On the left hand side of Figure 16, we show possible parameter variations on the PW model that obey the strict bounds. Note that the range of G values between the bounds is not covered by parameter variations. Approximating the uncertainty in the data with the current formulation of the model using a parametric methodology gives a very lower bound on the uncertainty.

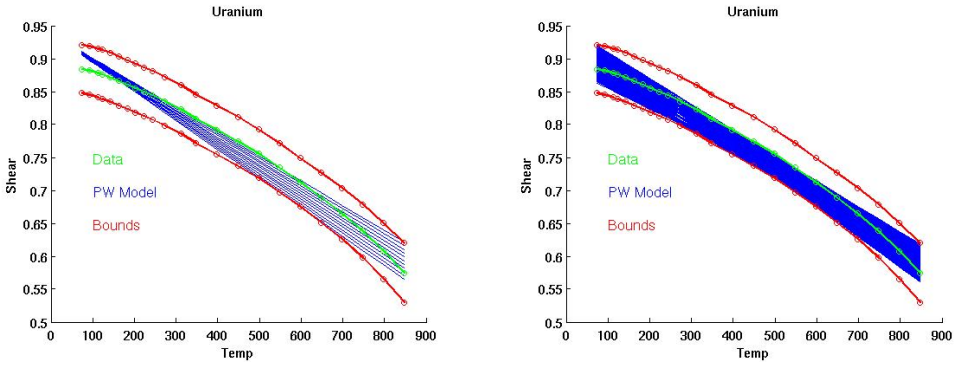

Figure 16: Uranium shear modulus versus temperature at $P = 0$; all curves as in previous figure. On the left, variations in the PW parameter α is shown as a family of blue lines. On the right we have possible variations that treat $G(\rho_0, T = 0)$ as a parameter, which implies no density dependence.

If we assume that we are modeling a system that remains at constant density under temperature variations (of course the thermal expansion coefficient is never zero), i.e. $G(\rho, T = 0)$=$G(\rho_0, T = 0)$, then we could model the uncertainty by treating $G(\rho_0, T = 0)$ as a parameter. This provides a slightly

improved lower bound, that may apply to a very limited number of engineered systems; see the right-hand side of Figure 16.

However, if we do not restrict ourselves to parameter variations, we can span the entire uncertainty by utilizing monotone and concave functional forms for the shear modulus at fixed density as a function of temperature; see Figure 17. Moreover, if physics category uncertainty is approached as a whole (i.e., the uncertainty of all physics processes that make up the physics category are considered simultaneously) the assumption of constant density can be dropped. This type of methodology will be described in Section 4.

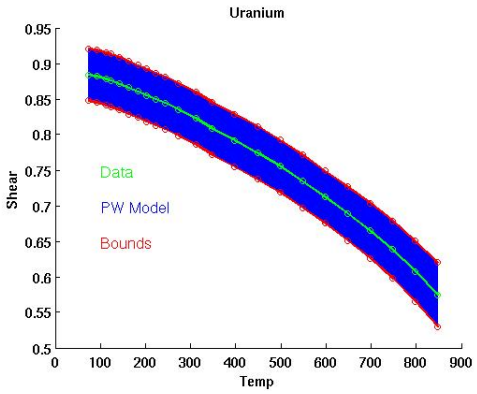

Figure 17: The entire uncertainty can be spanned using monotone and concave functional forms for the shear modulus.

Finally, for the third example we turn to the one-parameter HM strain-to-fracture model. In Figure 18 we show newly acquired strain-to-fracture data on a stainless steel, namely SS 1018, as a function of triaxiality. Recall (from Section 2.2) that the Hancock-Mackenzie model assumes that the strain to fracture is inversely proportional to the growth rate, an assumption based on observation, and that no appreciable plastic flow occurs prior to void nucleation. Moreover, the seminal Hancock-Mackenzie paper "On the mechanisms of ductile failure in high-strength steels subjected to multi-axial stress states" focuses on developing a strain-to-fracture model for steel. Therefore, Hancock-Mackenzie should be a relatively high-fidelity model for Stainless Steel. We do not know if the uncertainty in the data is aleatoric (i.e. due to lot-to-lot variations in the metal samples) or epistemic (which could be reduced with more samples) [44].

In Figure 18 (left), the red plus signs represent the data variations. A precise study of these data (and uncertainty) is in progress at Los Alamos National Laboratory.

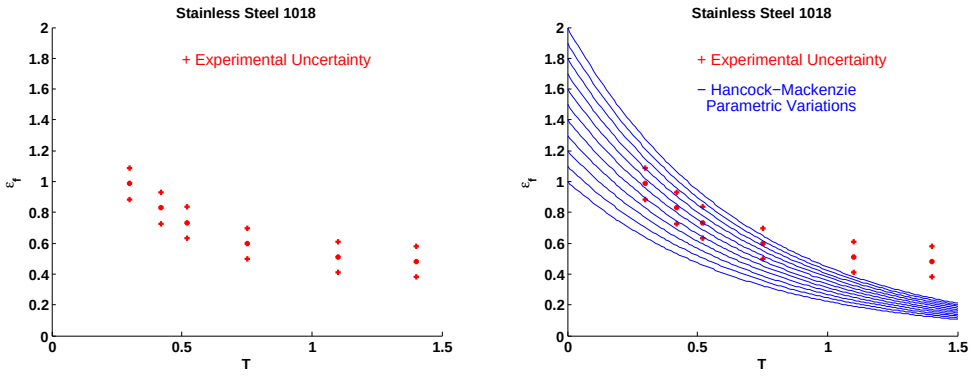

Figure 18: Hancock-Mackenzie parametric variations cannot span the uncertainty in the data.

In Figure 18 (right) compares parametric variations of the Hancock-Mackenzie model with strain-to-failure data, including experimental uncertainties, on 1018 Stainless Steel. Within the parameter variations several reasonable fits to the data can be obtained (note different fits can be obtained by weighting the data). However, the parameters do not span the uncertainty seen in the data. In fact,

$\hat{\mathcal{Y}} = \emptyset$. One can still define a $\hat{\mathcal{X}} \not\subseteq \mathcal{Y}$, but it will not provide lower or upper bounds on the uncertainty (see Figure 4).

It is important to emphasize that we selected the Maxwellian, Preston-Wallace, and Hancock-Mackenzie models for illustration purposes because they are based on simple approximations, with easy to describe assumptions, and they are three of the few models for which we have significant data (although, for Preston-Wallace only at nominal density). Moreover, their approximations are easy to articulate. Most of the functional approximations that make up physics models are complex and are, generally, the main content of the academic paper on the model moreover, very few are fits to data. This is true even when the functional form of the model is relatively simple. For instance, as mentioned above, the Hancock-Mackenzie model is based on a functional form that is a theoretical approximation (a spherical void in a perfectly plastic metal where no significant plastic flow occurs prior to void nucleation) derived in [28]. There are no parameters to absorb the uncertainty associated with these approximations. In general, Hancock-Mackenzie is used in conjuction with the Binary flow stress degradation model, a physics model with no parameters that is based on the gross approximation that flow stress does not degrade until strain-to-failure occurs. Again, there are no parameters to make up for this (very poor) approximation. In general, physics models are complex sets of non-independent assumptions and approximations that are integral to the fidelity of the model (see Section 2). It is these approximations and assumptions that dominate the uncertainty and there are no parameters with which to quantify the impact of these on our QoI.

Eliminate dependence of q_N on some of the q_i. The approximations underlying the Steinberg-Cochran-Guinan strength model described in Section 2.3 include, in particular, no strain-rate dependence. Therefore, it can be a low-fidelity model for simulating engineered systems where the strain rate undergoes significant change. The impact of the no-rate-dependence approximation in the Steinberg-Cochran-Guinan model clearly depends on the range of strain-rates being simulated and the QoI. An uncertainty quantification study on Steinberg-Cochran-Guinan should be able to quantify the impact of this lack of fidelity on a particular QoI for the given engineered system. However, this uncertainty clearly cannot be represented with parametric variation because the model is simply not strain-rate dependent. In fact, when applying a parametric methodology to systems with large strain-rate variations, almost surely, a higher uncertainty will be attributed to a physics model with higher fidelity (rate dependent) than will be attributed to Steinberg-Cochran-Guinan. Similarly, the approximations of the Hancock-Mackenzie damage model described in Section 2.1 include no temperature or strain-rate dependence. For all these cases, $\hat{\mathcal{Y}} = \emptyset$ and $\hat{\mathcal{X}} \not\subseteq \mathcal{Y}$.

3.1.3 There are no parameters for regimes with no data or reliable theory

Physics model parameters are introduced to provide a sufficiently accurate representation of the physics, but this is possible only where a mature theory and/or accurate data, experimental and/or numerical, are available at the time of model construction. Consequently, model parameters may be divided into subsets associated with specific regimes (limited temperatures, pressures, strain rates, etc.) where the physics is sufficiently well known. Although it is beyond the scope of this paper to enumerate and explain the approximations and assumptions that went into the development of every physics model presented in Section 2, we can select from Section 2, and elsewhere, many examples where there are no model parameters for regimes where no mature theory exists, the accuracy of the approximations are unknown, and/or there are no accurate data. Even if there are several models for the given physics process, none of them are reliable in such regimes. Neither parametric nor model selection methodologies can be meaningfully applied if the engineered system accesses these regimes. On the other hand, as will be dicussed in Section 4, general theoretical considerations or new data, even with large error bars, may still be used to place bounds on the physics.

There are no parameters in regimes where there are no data or reliable theory. Such regimes require either extrapolation from or interpolation between regions where the model has a sound experimental and/or theoretical foundation. We now consider examples of models that do not have the parameters needed to accurately represent specific physics regimes, and therefore entail either extrapolation or interpolation.

Extrapolation

Consider again the PW model of the shear modulus as a function of temperature. With the goal of improving model fidelity beyond that of the simple PW model, a modeler might find a complex parameterized functional form that exactly fits the mean of the data for a large set of metals at $P = 0$. However, it is entirely possible, perhaps probable, that the error in G when extrapolating to higher pressures is greater for this complex relation than it would be for the original, linear approximation. Moreover, there is no reason that the parameters of this complex functional form, found by optimizing across metals, would span the range of G values between the Hashin-Shtrikman bounds. Finally, variations in the parameters of a complex functional form could easily violate the physical constraints on the shear modulus as a function of temperature, i.e. concavity and monotonicity (in the absence of phase-change). We will now show that not only are there, in general, no physics model parameters that can be used to statistically absorb the assumptions or the approximations of a particular physics model, but that when this is attempted unanticipated things can happen when extrapolating the model to other regimes.

For instance, the data in Figure 18 is taken at room temperature. The Hancock-Mackenzie (HM) model can be modified so that it can be extrapolated to lower or higher temperatures. Since the strain-to-fracture, ϵ_f, increases with T, this can be accomplished by including a factor of the form $1 + pT^*$ where $p \geq 0$ and $T^* = (T - T_{RT})/(T_m - T_{RT})$, where T_{RT} = room temperature. Consequently, the room-temperature uncertainties become larger (smaller) at higher (lower) temperatures. It is perhaps reasonable that the uncertainty increases when we extrapolate to regimes without data, but when the uncertainty contracts in extrapolation we suspect that we are doing something wrong. The authors have seen this artificial, extrapolation-induced expansion and contraction of parametric uncertainties for much more complicated physics models dominate the uncertainty quantification.

Interpolation

The Preston-Tonks-Wallace (PTW) constitutive relation is based on low- and high-rate sub-models for which there are accurate experimental data and reliable theory. At low rates we have Hopkinson bar and mechanical test system data, while at very high rates we have strong shock Hugoniot data. These data constrain the uncertainty in the flow stress to roughly $\pm 10\%$ in both limits. There are no reliable data for intermediate strain rates from 10^4 s^{-1} to 10^9 s^{-1}, hence the PTW model was constructed without parameters to control the flow stress at these rates; the model simply interpolates between the low- and high-strain-rate limits. Because of the model form, parametric variations consistent with the data can change the PTW flow stress by only $\pm 10\%$ at intermediate rates. However, a new dislocation-dynamics-based model predicts flow stresses significantly above the PTW bounds at intermediate rates [43]. Therefore, $\hat{\mathcal{Y}} = \emptyset$ and $\hat{\mathcal{X}} \not\subseteq \mathcal{Y}$.

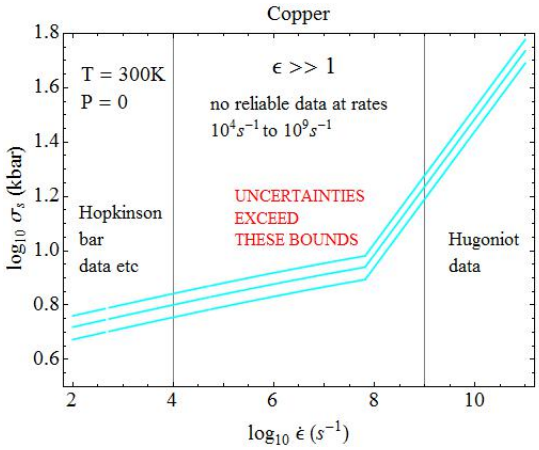

Figure 19: PTW saturation stress versus plastic strain rate.

The uncertainty in the flow stress cannot be covered with parametric variation because the parameters were not provided for that purpose, but instead to distinguish between the mean behaviors of different metals given a set of assumptions and approximations. The parameters of many physics models are provided for the same reason. To list some examples from Section 2: the JWL HE EOS, Johnson-Cook Damage, Hancock-Mackenzie strain-to-failure, TEPLA, Johnson-Cook Flow Stress, Preston-Wallace shear modulus, Burakovsky-Greeff-Preston shear modulus, Straub shear modulus, Steinberg-Cochran-Guinan,

and DSD HE burn.

3.1.4 Parameters are designed to capture mean behavior

In this subsection we provide two examples illustrating our point that physics models are often constructed to capture mean behavior, but then the model parameters cannot be varied to cover the uncertainty seen in the data. Even unrealistic parameter variations will generally not cover this uncertainty.

Our first example concerns prompt fission neutron spectra (PFNS). In Subsection 3.2.2 we showed that the Maxwellian model parameter cannot be used to account for the experimental uncertainty. In this Section, we show that the more sophisticated Watt and Madland-Nix models do not have parameters that can span the uncertainty. Both the Watt and Madland-Nix models assume functional forms that are approximations to the true physics. In Figure 20, again we have normalized PFNS data to a Maxwellian and we show parametric variations of the Watt model. Notice that at low energies the parametric variations cannot span the uncertainty in the data. This is because the theorists did not provide parameters to span the data, rather the parameters are designed to move between like processes (e.g., Pu239 and U235) and to approximate the mean behavior of the physics process.

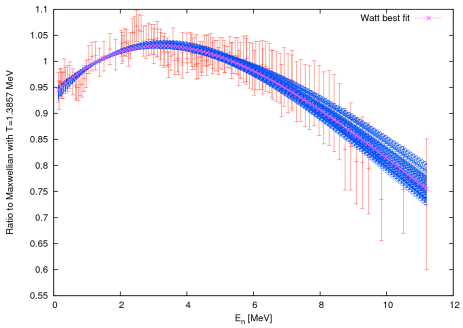

Figure 20: Prompt Fission Neutron Spectrum data normalized to a Maxwellian

Note that, since PFNS is a pdf, the integral of the spectrum must be one. Both the Watt model and the Madland Nix model obey this constraint and the result is that parametric variations in either model cannot account for the uncertainty in the data for low energies.

Our second example is the Preston-Wallace Finite T physics model. The parameter in the Preston-Wallace finite T physics model is clearly designed to move between like processes (e.g., Uranium and Copper) and approximate the mean behavior of the physics process.

3.2 Combined model selection and parametric methodologies

The difference between available physics models often exceeds the difference that can be achieved using the parameters of the individual physics models. If the models are considered to be of equal fidelity, this is another clear indication that parametric methodologies can provide at best a lower bound on uncertainty. When this is known, a model selection methodology (switching out available calibrated models) is an alternative to applying a parametric methodology for estimating uncertainty. Alternatively, parametric and model selection methodologies can be combined. However, such hybrid methodologies have their shortcomings: areas of uncertainty are left unexplored, and they provide only lower bounds on uncertainty.

Unexplored areas of uncertainty

Let us first consider the three flow-stress degradation models of Section 2.1: Binary, Linear, and Cochran-Banner. Of these physics models, only Cochran-Banner is parameterized. We will show that these models and their available parameters do not overlap leaving a subspace of potential uncertainty unexplored. The three models are shown in Figure 21; the fine magenta lines indicate parametric variations on the Cochran-Banner model. Figure 21 shows that the three models degrade the flow-stress quite differently as damage accumulates. Therefore, for loading conditions that result in a high ratio of cumulative strain (ϵ) to fracture strain (ϵ_f) (see Section 2.1), a model selection methodology over these three models (we temporarily assume no variations in D_0) will likely result in three very different values for a given output

QoI. There are large disjoint domains in the first quadrant of the $D - \mathcal{F}$ plane (recall that $\sigma = \sigma_0 \mathcal{F}(D)$) that are inaccessible by the models. In general, we denote the union of all such disjoint domains by $\mathcal{D}$.

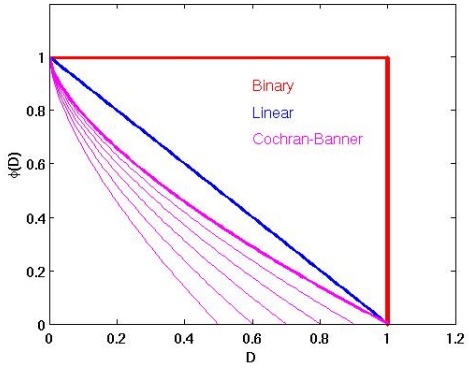

Figure 21: Comparison of the Binary (red), Linear (blue), and Cochran-Banner (magenta) flow stress degradation models. The various magenta curves correspond to different values of D_0.

As another example, Figure 22 illustrates the differences in saturation stress as a function of strain rate between the PTW, Steinberg-Cochran-Guinan, and Johnson-Cook flow stress models. Theoretical and experimental uncertainties for the models are indicated by dashed lines. The black vertical line at $10^4 s^{-1}$ indicates the highest rates for which we have stress-strain data. The dashed lines represent parametric uncertainty for the flow stress models that are consistent with the available data. Clearly, applying a model selection methodology over these three models will result in a higher uncertainty than applying a parametric methodology to any individual model. Note that these models, including parameter variations, do not overlap leaving a large sub-space, $\mathcal{D}$, of potential uncertainty unexplored. Here $\mathcal{D}$ is a consequence of the models being constructed under different assumptions and in regimes where there is no experimental data or reliable theory. Moreover, a combined parametric and model selection methodology will result in a discontinuous space.

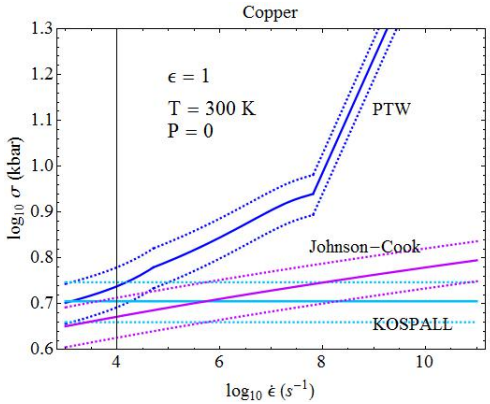

Figure 22: Flow stress versus strain rate for the PTW, Steinberg-Cochran-Guinan, and Johnson-Cook strength models. The dashed lines indicate $\pm 10\%$ uncertainty in σ.

3.2.1 In some cases, combined methodologies provide only lower bounds on uncertainty

Assume there exists another flow stress degradation model, X, that lies in the $\mathcal{D}$ of the Linear, Binary, and Cochran-Banner models. We further assume that all four models are of equal fidelity and therefore should all be included in the uncertainty analysis. We now make a very important point. Although the $\mathcal{F}(D)$ of model X is between that of two of the other models, it does not follow that the QoI of X is between the QoIs of the other two models. In other words, it is often, although certainly not always, incorrect to assume monotonicity (an assumption that can be quite complicated to define when the

support is a function space). It is clear that an analysis based on the original three models alone could yield an uncertainty in the QoI that is less than that obtained when model X is included, even though X lies between the other models. If monotonicity cannot be established and a set of models cannot be refuted, a model selection uncertainty analysis provides only a lower bound on the QoI uncertainty.

We now discuss an example from the material strength category. Recall, from Section 2, that the strength physics category is modeled with a composite continuum level model that requires physics models for four distinct physics processes. Extensive parametric studies to date have focused on zero-pressure data and the construction of priors for the dimensionless parameters of the PTW model. Although PTW must be used in conjunction with a model for the shear modulus (flow stress = $G \times$ scaled PTW stress), no attempt has been made to address uncertainty associated with the density dependence of G. This is a serious shortcoming: for lack of experimental data, the uncertainty associated with $G(\rho)$ is much greater than the uncertainties in the PTW parameters; thus the composite model uncertainty is much greater than that of PTW alone.

Here we consider two models for $G(\rho, T = 0)$ namely the Straub and BGP (Burakovsky-Greeff-Preston) models, and compare the parametric uncertainties in the flow stress of copper, which we take to be pressure independent, with the uncertainty due to the difference between the Straub and BGP models. In Figure 23, one can see that the difference between the two shear modulus models for copper makes an order of magnitude larger contribution to the plastic flow uncertainty than the parametric uncertainties. If linearity is assumed, a parametric methodology would underestimate the uncertainty in the flow stress of Cu by an order of magnitude. Clearly, a model selection methodology would produce a more realistic bound on our confidence.

Unfortunately, as a specific physics phenomenon becomes better understood (experimental evidence and theoretical advances increase) more models are developed and model selection methodologies can yield increasing uncertainties on a calculated QoI. This is a clear indication that, like parametric methodologies, model selection methodologies only provide, at best, a lower bound on the uncertainty.

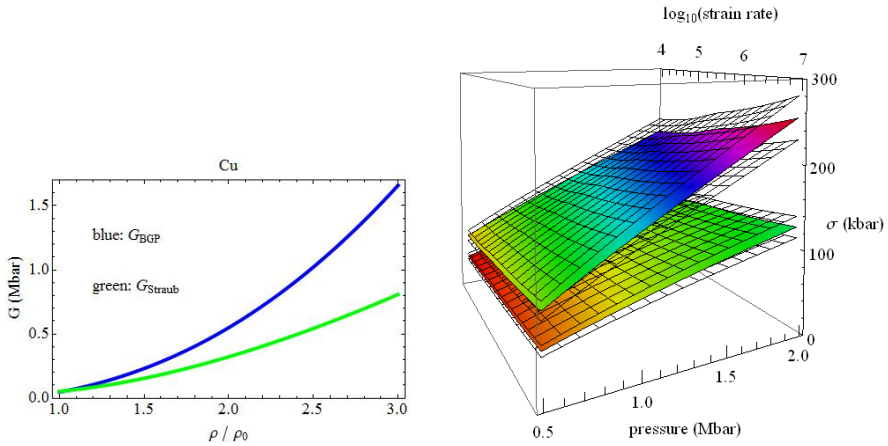

Figure 23: Left: Comparison of the Burakovsky-Greeff-Preston (BGP) and Straub (S) models for the density dependence of the shear modulus. Note that the BGP model predicts the higher, hence larger flow stress at high pressures. Right: Comparison of PTW CU flow stresses using the BGP (upper surfaces) and S (lower surfaces) models for G. The transparent surfaces are 10% parametric uncertainties (a known uncertainty from small scale experiments at nominal densities)

.

Finally, the parametric uncertainties in Figure 23 determined at nominal densities result in larger uncertainties on flow stress if the BGP model is used in conjuction with PTW than if the Straub model is used. This is because the distance between the uncertainty bounds will expand/contract in proportion to G, which is simply larger for the BGP model.

We have shown that the difference between available physics models often exceeds the difference that can be achieved using the parameters of the individual physics models. This is due to the unique set of approximations and assumptions made by the individual physics models. The validity of the approximations and assumptions over a regime (e.g., range of strain rates) of interest for a given physics model represents our lack of knowledge of the physical process.

4 Physical uncertainty bounds

Both parametric and model selection methodologies suffer from a common, serious shortcoming, namely, they are linked to the existing suites of models available in each of the physics categories pertinent to a given system. Each of those models is constructed on the basis of simplifying assumptions and approximations (chosen functional forms, analytic approximations, extrapolations, ...) that are specific to that model, and as emphasized above, the models, and certainly the composite models, in a physics category can vary significantly. Parametric analyses are clearly inadequate as they are model specific, hence they do not account for different physics approximations. Model selection methodologies essentially amount to quantifying the variation in calculated system performance over the existing set of approximations employed in a given physics category, and therefore provide only a lower bound on the uncertainty in calculated performance. However, we can do much better than this: we can bound the physics. Subject matter experts in a particular physics category could bound the physical quantities returned by the models and sub-models in that category. In contrast to the model selection and parametric methodologies, this approach would provide upper bounds on simulated system performance.

Bounds can be placed on a physical quantity in a given regime by means of experimental data, numerical data, or fundamental theory. Experiment, simulation, and theory are generally each reliable only for limited spatial and temporal scales, and for restricted ranges of density, temperature, energy, strain rate, etc. Since a model or sub-model might span several regimes, the bounds will typically be set by both data and theory. Reliable experimental data and the associated uncertainties should be used to bound the physics whenever available. Some models or sub-models represent physical processes that are experimentally inaccessible because they occur at very small spatiotemporal scales, or involve extreme pressures, temperatures, etc. In these cases, simulations might be carried out to generate numerical data with error bars. Relevant simulation techniques/codes include classical molecular dynamics (MD), quantum MD, electronic structure codes, particle-in-cell codes (plasmas), dislocation dynamics codes, DNS simulations (fluids), and hydrocode simulations. This approach to bounding the physics will become progressively more viable as computing systems advance toward the exascale (although, we are performing QMD calculations now). Finally, we have recourse to fundamental theory. Here the strategy is to draw on general principles of modern theoretical physics and our understanding of particular physical processes to place bounds on the physical quantities associated with the given process. It is important to point out that there is no general prescription for carrying out this program; it must be done on a case-by-case basis. Nevertheless, we can garner insight into the general procedure by considering a specific example, namely, material strength at intermediate plastic strain rates and large strains, where there are no direct measurements and no simulation results. The strength (flow stress) at plastic strain rates exceeding roughly $10^4 s^{-1}$ is controlled by both dislocation-dislocation intersection, which usually results in the formation of a so-called crossed state (two dislocations pinned together at their intersection point) with a finite lifetime, and viscous phonon drag. Note that we are interested in placing bounds on the strength from ambient to very high pressures. The mean lifetime of the crossed state can be bounded using calculated (quantum MD) values of the shear modulus, and extreme values of the dislocation density ($10^6 cm^{-2}$ to $10^{12} cm^{-2}$). The dislocation drag coefficient, B, has been measured for a large number of metals; we would employ the maximum and minimum values. The aforementioned quantities can be combined (Orowan relation) to give the upper and lower bounds on the flow stress as a function of the plastic strain rate at intermediate rates where there are no data and no simulation results.

It should be stressed that bounds on the physics do not constitute a model. Bounding does not involve the introduction of parameters, as in model construction, hence standard parametric or model selection methodologies are inapplicable. We now outline several approaches that either have, are, or could be taken to bound the physics in the material damage and strength categories. For other physics categories we defer to the SMEs in those subject areas.

4.1 Material Damage

If material damage is characterized by a single positive scalar field D (though, in general, tensors are required), e.g. the porosity in a ductile metal, or the crack density in brittle materials, it is trivial to place extreme, but unrealistic, bounds on the flow stress degradation: for D normalized to unity, the upper bound is the full flow stress for $D < 1$ and zero for $D = 1$, while the lower bound is the full flow stress for $D = 0$ and zero for $D > 0$. However, narrower, more realistic bounds are preferable. In principle, direct measurements of the flow stress of damaged material could be carried out, though in

practice it may be problematic to obtain samples with uniform damage. Simulations to determine the strength of materials with both void and crack damage could certainly be carried out. Finally, upper and lower bounds can be placed on the flow stress by employing the methods of effective medium theory, which applies to composite or multi-phase materials.

4.2 Strain to Fracture

Bounds on the fracture strain as a function of temperature and strain rate are most reliably obtained from experiment when possible, e.g. standard tensile testing. The fracture strain is sensitive to impurity content and material processing, and since fracture is inherently stochastic, uncertainties (error bars) are expected to be relatively large. Bounds on the fracture strain might be determined through a combination of the theories of void growth (ductile metals) and crack propagation (brittle materials), numerical simulations, and percolation theory, which captures the effects of material connectivity and could be used to determine the porosity or crack density at which material fracture takes place. A theoretical/computational approach is likely the only means of bounding the fracture strain at very high strain rates ($\geq 10^4 s^{-1}$), elevated pressures, or both.

4.3 Shear Modulus

Composite material strength models include sub-models for the shear modulus, G; in general, these must be multi-phase models. As shown in Figure 23, our current models for G can diverge dramatically with increasing pressure, implying large uncertainties in G at high pressures. However, with the exception of the BGP model, these models are outdated. Today we can carry out very reliable quantum molecular dynamics (QMD) calculations of G as a function of pressure and temperature for multi-phase materials. In summary, the approach is as follows. Given the phase diagram, we calculate the requisite single-crystal elastic constants for each crystal structure over a pressure-temperature grid, evaluate the Hashin-Shtrikman bounds on G for each point, and average to give G. The G values and bounds can be used in tabular form, or an analytic fit can be obtained. The calculation of each single-crystal elastic constant entails five crystal-energy calculations (the curvature of a quadratic fit gives the elastic constants), each of which can take several weeks, and a large number of single-crystal constants are needed in low-symmetry structures. Such QMD calculations are now under way for several materials.

4.4 Melt Temperature

The melt temperature depends on both crystal structure and pressure for a given structure. The solid-liquid equilibrium boundaries for several candidate crystal structures of a multi-phase material can be calculated by means of QMD. The structure with the highest solid-to-liquid transition temperature over some pressure interval is the stable phase along the melting curve in that interval. In general, these individual solid-liquid boundaries are concave down and intersect. The physical melting curve is the envelope of these boundaries, and the intersection points on the melt curve are solid I - solid II - liquid triple points. Bounds on the melt temperature can be estimated from the QMD code output; uncertainties are typically a few percent. Moreover, the Clausius-Clapeyron relation provides the slopes of the solid I - solid II phase boundaries at the triple points. Thus the high temperature phase diagrams of metals, alloys, and compounds can be mapped out by means of QMD simulations; see Figure 24.

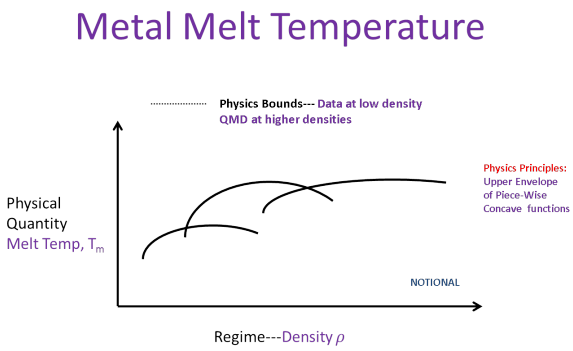

Figure 24: Bounding the density-dependent melting temperature with QMD. The black curves are solid-liquid equilibrium boundaries for different candidate crystal structures. The envelope of these boundaries is the physical melting curve.

4.5 Flow Stress

We refer the reader to the above discussion of flow stress at strain rates exceeding roughly $10^4 s^{-1}$, and at all pressures, where there are no simulation results and no direct measurements. At rates under $10^4 s^{-1}$ and essentially zero pressure, the flow stress can be bounded using accurate stress-strain data from mechanical testing apparatus and Hopkinson bars, but there are no techniques available to measure high-pressure strength at these rates, nor are numerical data available. Again, we must rely on theory, in this case dislocation dynamics, to provide bounds on the flow stress.

5 Concluding remarks

The primary purpose of this paper was to motivate the need for a new methodology for determining upper bounds on the uncertainties in simulations of engineered systems due to limited fidelity in the composite continuum-level physics models needed to simulate the systems. This paper has shown that current methodologies – parametric and model selection – cannot quantify this uncertainty. In particular, we have shown that some models have no (or almost no) parameters to vary. Moreover, parameters in a physics model are generally provided to move between like processes (e.g. copper and aluminum) and model mean behavior. Therefore, parameters in physics models have little, if anything, to do with the approximations for a given model. Generally no parameters are provided in regimes where there are no data to use to move between like processes. Finally, we show that combining model selection and parametric methodologies lead to disjoint domains and like parametric methodologies provide, at best, a lower bound on the uncertainty. Nineteen physics models from five physics categories (plasma fusion, material damage, neutronics, material strength, and high explosives) were used to illustrate these points. Finally, we propose obtaining bounds on simulation uncertainties by first determining bounds on the physical quantities or processes relevant to system performance. Physics bounds are currently being constructed and use combinations of fundamental physics, experimental data, and numerical data. Some of the bounds currently being worked on were briefly discussed. Papers containing much more detail for individual bounds are being written, by the authors and others.

6 Appendix A

Represent each of the physical quantities $\{q_i\}$, $i = 1, \ldots, N$, by a point. If q_n is a function of q_m (and possibly other q_i) then connect the points q_m and q_n by a line segment directed from q_m to q_n. The physics processes and physics categories are encoded in the resulting directed graph. The subset of vertices with one or more edges directed into them are the physical quantities defining the physics processes. The physics categories are enumerated by the following procedure. First, it may be that two or more vertices are connected by two oppositely-directed edges; e.g., material strength depends on material damage but damage evolution depends on strength. Such closed loops must be removed from the digraph to determine the physics categories. A physics process with no edges directed out of it immediately identifies a physics

category. The physics category associated with such a vertex, say q_{c1} (c $\sim$ category), is comprised of q_{c1} plus the $n-1$ physics processes, q_{cj}, on directed paths terminating on q_{c1}; this physics category consists of n physics processes and is defined by q_{c1}. Next, delete all such physics categories from the digraph. The vertices of the resulting (possibly disjoint) graph have only inwardly-directed edges and as such identify the remaining physics categories.

References

[1] National Research Council. Assessing the Reliability of Complex Models: Mathematical and Statistical Foundations of Verification, Validation, and Uncertainty Quantification. Washington, DC: The National Academies Press, 2012.

[2] T.G. Trucano, L.P. Swiler, T. Igusa, W.L. Oberkampf and M. Pilch, Reliability Engineering and System Safety **91**, 1331 (2006)

[3] D.E. Vaughan and Dean L. Preston, Los Alamos National Lab, LA-UR-14-20441.

[4] M.C. Kennedy and A. O'Hagan, J.R. Statist. Soc. B **63**, 425 (2001)

[5] D.G. Madland and J.R. Nix, Nucl. Sci. Eng **81**, 213 (1982)

[6] B.E. Watt, Phys. Rev. **87**, 1037 (1952)

[7] D.G. Madland, Heavy Ion Phys. **10**, 231 (1999)

[8] G. Zwicknagel, Nucl. Instrum. Methods Phys. Res., Sect. B **197**, 22 (2002)

[9] M. Ahsan Zeb, J. Kohanoff, D. Sa'nchez-Portal, A. Arnau, J.I. Juaristi, and E. Artacho, Phys. Rev. Lett. **108**, 225504 (2012)

[10] Z.-H. Hu, Y.-H. Song, and Y.-N. Wang, Phys. Rev. E **82**, 026404 (2010)

[11] J.D. Huba, *NRL Plasma Formulary* (Naval Research Laboratory, Washington, DC, 2009)

[12] C.-K. Li and R.D. Petrasso, Phys. Rev. Lett. **70**, 3059 (1993)

[13] A.A. Solodov and R. Betti, Phys. Plasmas **15**, 042707 (2008)

[14] G. Zwicknagel and C. Deutsch, Phys. Rev. E **56**, 970 (1997)

[15] L.S. Brown, D.L. Preston, and R.L. Singleton, Jr., Phys. Rep. **410/4**, 237-333 (2005)

[16] Private Communication with D.N. Preston and L. Hill, HE Experimentalist

[17] P.E. Grabowski, M.P. Surh, D.F. Richards. F.R. Graziani, and M.S. Murillo, Phys. Rev. Lett. bf 111, 215002 (2013)

[18] D.A. Liberman, Phys. Rev. B **20**, 4981 (1979)

[19] L. Burakovsky and D.L. Preston, J. Phys. Chem. Solids **65**, 1581 (2004)

[20] D.L. Preston, D.L. Tonks, and D.C. Wallace, J. Appl. Phys. **93**, 211 (2003)

[21] G.K. Straub, Elastic Shear Modulus: Fits to Data and Extrapolation to Large Compressions and Negative Pressure, LA-11806-MS (1991)

[22] L. Burakovsky, C. Greeff, and D.L. Preston, Phys. Rev. B **67**, 094107 (2003)

[23] D.C. Wallace, Phys. Rev. B **24**, 5607 (1981)

[24] A.M. Fraser, Constraining Uncertainty with Laws of Physics (2013). LA-UR-13-21824.

[25] J.W. Hancock and A.C. MacKenzie, J. Mech. Phys. Solids **24**, 147 (1976)

[26] G.R. Johnson and W.H. Cook, Int. J. Eng. Fract. Mech. **21**, 31 (1985)

[27] J.N. Johnson and F.L. Addessio, J. Appl. Phys. **64**, 6699 (1988)

[28] J.R. Rice and D.M. Tracey, J. Mech. Phys. Solids **17**, 201 (1969)

[29] S. Cochran and D. Banner, J. Appl. Phys. **48**, 2729 (1979)

[30] K.G. Hoge and A.K. Mukherjee, J. Mat. Sci. **12**, 1666 (1977)

[31] D.J. Steinberg, S.G. Cochran, and M.W. Guinan, J. Appl. Phys. **51**, 1498 (1980)

[32] G.R. Johnson and W.H. Cook, *Proc.* 7^{th} *Int. Symp. Ballistics*, Am. Def. Prep. Org. (ADPA), Netherlands (1983)

[33] F.J. Zerilli and R.W. Armstrong, J. Appl. Phys. **61**, 1816 (1987)

[34] P.S. Follansbee and U.F. Kocks, Acta Metall. **36**, 81 (1988)

[35] D.J. Steinberg and C.M. Lund, J. Appl. Phys. **65**, 1528 (1989)

[36] J.S. Langer, E. Bouchbinder, and T. Lookman, Acta Mater. **58**, 3718 (2010)

[37] E. Voce, J. Inst. Met. **74**, 537 (1947/48)

[38] D.L. Preston and D.C. Wallace, Solid State Comm. **81**, 277 (1992)

[39] J.B. Bdzil and D.S. Stewart, Phys. Fluids A **1**, 1261 (1989)

[40] C.L. Mader, Detonation Properties of Condensed Explosives Computed Using the Becker-Kistiakowski-Wislon Equation of State, Los Alamos Scientific Laboratory report LA-2900 (1963); FORTRAN BKW: A Code for Computing the Detonation Properties of Explosives, Los Alamos Scientific Laboratory report LA-3704 (1967)

[41] J.W. Kury, H.C. Hornig, E.L. Lee, J.L. McDonnel, D.L. Ornellas, M. Finger, F.M. Strange, and M.L. Wilkins, Proc. 4th Symposium on Detonation, Office of Naval Research (1965); E.L. Lee, H.C. Hornig, and J.W. Kury, Lawrence Livermore Laboratory report UCRL-50422 (1968); E. Lee, M. Finger, W. Collins, JWL Equation of State Coefficients for High Explosives, Lawrence Livermore Laboratory report UCID-16189 (1973)

[42] G. Simmons and H. Wang, Single Crystal Elastic Constants and Calculated Aggregate Properties: A Handbook (The MIT Press, Cambridge, MA, 1971)

[43] A. Hunter and D.L. Preston, Analytic model of the remobilization of pinned glide dislocations from quasi-static to high strain rates, Int. J. Plasticity (2015), http://dx.doi.org/10.1016/j.ijplas.2015.01.008.

[44] S.R. Chen, private communication